Electronic Thesis and Dissertation Repository

8-22-2024 1:00 PM

Revealing role of PGC1-alpha in chondrocyte and knee joint health

Yuri Kim,

Supervisor: Frank Beier, *The University of Western Ontario*
A thesis submitted in partial fulfillment of the requirements for the Master of Science degree in Physiology and Pharmacology
© Yuri Kim 2024

Follow this and additional works at: https://ir.lib.uwo.ca/etd

Recommended Citation

Abstract

Osteoarthritis is a common chronic disorder of joints which leads to the reduction of articular cartilage and pain. This research depicts the function of peroxisome proliferator-activated receptor-gamma coactivator 1-alpha (PGC1α) in chondrocytes that maintains mitochondrial function and its role in OA pathogenesis. We analyzed the impact of the PGC1α inhibitor SR-18292 in gene expression and mitochondrial function using immature murine articular chondrocytes (IMACs) in primary culture. There was an important and marked downregulation of mitochondrial-related genes (Esrra, Nrf1, Tfam) in response to SR-18292 treatment, as indicated by quantitative real-time PCR and RNA sequencing studies. Additional fluorescence imaging showed markedly decreased mass and mitochondrial membrane potential. These findings reinforced the premise that PGC1α had a key role in maintenance of mitochondrial health in chondrocytes and that its inhibition may drive OA development.

Keywords

Summary for Lay Audience

Osteoarthritis is a common disease in the joint. It's caused by the wearing of a protective cushion at the ends of bones located in a joint, causing pain and movement limitation. However, despite its prevalence, effective therapies for OA are lacking, largely because the precise biological processes driving the disease remain to be fully understood. This study aimed at the special protein PGC1α; it is known to play a critical role in the maintenance of mitochondrial health, the energy powerhouse, in cartilage.

Mitochondria are the energy suppliers for normal cellular activities; thus, any disturbance in this activity may lead to cellular damage or diseases. The study was designed to define changes happening in chondrocytes that occur when activity of PGC1α is pharmacologically inhibited by a small molecule known as SR-18292. The aim was to understand whether impairing mitochondrial function in cartilage cells contributes to the development of OA.

We treated chondrocytes from mice with SR-18292 and observed changes in gene activity and mitochondrial function. Our experiments showed that in case PGC1α is not able to work, the activity of genes responsible for the maintenance of mitochondria health drops. It means that mitochondria presented in these cells are not working properly. Subsequent experiments, using special dyes which fluoresce when they interact with healthy mitochondria, showed that both the amount and the function of the mitochondria were reduced in treated cells.

Such findings are important in the respect that they give a clearer picture of how mitochondrial dysfunction in chondrocytes may contribute to the progression of OA. An understanding of these processes allows for new opportunities for treatment. For example, it might become possible to delay or prevent the process leading to cartilage degradation in OA through therapeutic activity using PGC1α, or by improving mitochondrial function.

Overall, the current study has identified the PGC1α importance in chondrocytes to sustain cellular health and brought mitochondrial dysfunction. This possibly suggests new therapeutic interventions that focus on these basic cellular processes will be developed, leading to improved management of the disease.

Acknowledgments

As I come to the final stage of my master's journey, I am profoundly aware of the many people whose efforts and support have made this accomplishment possible. First and foremost, I would like to extend my deepest gratitude to my supervisor, Dr. Frank Beier. Your constant consideration for your students and your willingness to offer both academic and personal support have been invaluable to me. Meeting a mentor like you has been an incredible stroke of luck. I have learned and experienced so much thanks to you.

I also wish to express my sincere thanks to my Advisory Committee members, Dr. Christopher Pin, Dr. Matthew Grol, and Dr. Ute Schwarz. Your feedback during our meetings was instrumental in guiding the direction of my research. I particularly enjoyed the process of learning the ChIP assay with the help of Dr. Christopher Pin, even though it did not make it into my final thesis. Dr. Matthew Grol's lectures in the MSK course were the most intriguing part of my studies, and I am grateful for the insightful advice you provided alongside your excellent teaching.

My heartfelt thanks go to the lab technicians, Dawn Bryce and Holly Dupis, whose support with experimental protocols and animal studies was indispensable. I could not have reached this point without your help. Dawn, our long-time friend in the lab, retired during my master's program, and I hope she is enjoying her well-deserved retirement from afar.

I am also grateful to my fellow lab members, Ermina Hadzic, Sepideh Taghizadeh, Emily White, and Jasleen Grewal. Thanks to you, I never felt alone or isolated while pursuing my master's degree abroad, and I truly enjoyed our time together in the lab. I would also like to thank Jeffery Hutchinson, Courtney Brooks, and Diana Quinonez from Dr. Seguin's lab for always making time to assist me whenever I needed help.

Finally, I would like to thank Magda, Emily, and Kiki for always be there to support my mental health and make me stay positive in any situation. I don't know what I would do without your positive vibes! I already miss you all. Also, my dear friends and family in Korea, thank you for all the night talks and being supportive no matter what I do. Thanks to your cheering, I was able to finish this journey.

There are many others to whom I owe thanks. Writing this acknowledgment has made me realize once again how much I have relied on the support and encouragement of so many individuals to complete my master's program successfully. I am deeply grateful to you all and wish you the best and happiness wherever you may be.

Table of Contents

List of Tables

List of Figures

List of Abbreviations

OA	Osteoarthritis
ECM	Extra cellular membrane
ER	Endoplasmic Reticulum
PGC1α	Peroxisome proliferator-activated receptor gamma coactivator 1-alpha
SOX9	SRY-Box Transcription Factor 9
MMPs	Matrix metalloproteinases
IMAC	
OXPHOS	Oxidative phosphorylation
mtDNA	Mitochondrial deoxyribonucleic acid
ETC	Electron transport chain
ATP	Adenosine triphosphate
ROS	Reactive oxygen species
BCL-2	B-cell lymphoma 2
OPA1	OPA1 Mitochondrial Dynamin Like GTPase
OMM	Outer mitochondrial membrane
IMM	Inner mitochondrial membrane
TFAM	Mitochondrial transcription factor A
NRF1	Nuclear respiratory factor 1
PPARα	Peroxisome Proliferator Activated Receptor alpha
AMPK	AMP-activated protein kinase
SIRT1	Sirtuin (silent mating type information regulation 2 homolog) 1
ESRRα	Estrogen-related receptor alpha
VEGFR2	Vascular endothelial growth factor receptor 2
PGC1β	Peroxisome proliferator-activated receptor gamma coactivator 1-beta
RT	Room temperature
P	Passage

DMSO	Dimethylsulfoxide
PCR	Polymerase Chain Reaction
Actb	β-actin
MPC1	Mitochondrial pyruvate carrier 1
KEGG	Kyoto Encyclopedia of Genes and Genomes
GO	Gene Ontology
GSEA	Gene Set Enrichment Analysis
DEG	Differential gene expression
CXCL13	B cell-attracting chemokine-1
PMAIP1	Phorbol-12-myristate-13-acetate-induced protein 1
POU2F2	POU class 2 homeobox 2
SLC22A3	Solute carrier family 22 member 3
FDR	False Discovery Rate
Ct	Threshold cycle
ANOVA	Analysis of Variance
PDK4	Pyruvate dehydrogenase lipoamide kinase isozyme 4
COL10a	Collagen Type X Alpha 1 Chain
SP110	Host transcription factor Speckled 110 kDa

List of Appendices

Chapter 1

1   Introduction

Osteoarthritis (OA) is the most common chronic joint disease caused by articular cartilage loss, subchondral sclerosis, and abnormalities of the synovial membrane and periarticular structures. It is characterized by pain, immobility, and greatly reduced quality of life (Cowan, 2010). Even though OA affects 1 in 3 people over age 65, current treatments for OA are unsatisfactory, largely because we do not understand the underlying molecular mechanisms very well and therefore don't have enough candidate targets for drug treatments (Wieland, 2005).

The pathogenesis of OA is characterized by extracellular matrix (ECM) degradation and cellular stress that led to the activation of proinflammatory cytokines or dysfunction of cellular organelles such as endoplasmic reticulum (ER), peroxisome, and mitochondria (Wu, 2014). Among the various cellular organelles, mitochondria are one of the most important organelles in eukaryotic cells. Mitochondria regulate important cellular functions and cell survival that may have a key role in age-related disease (Srivastava, 2017). Recent studies suggested that the dysfunction and degradation of mitochondria could be associated with OA (Zheng, 2021). Thus, finding key triggers of mitochondrial dysfunction in cartilage degeneration may help to define treatment strategies for OA and other joint or cartilage disorders.

Peroxisome proliferative-activated receptor gamma coactivator 1 alpha, PGC1α, is known as a key regulator of energy metabolism, stimulates mitochondrial biogenesis and promotes the remodeling of muscle tissue (Flachs, 2005). PGC1α is highly expressed in oxidative tissues such as heart, muscle, kidney, and brain (Cheng, 2018). It is a positive regulator of mitochondrial biogenesis and respiration, and altered expression or activity of PGC1α has been reported in several disorders associated with oxidative stress, including Parkinson's disease, Alzheimer's disease, and Huntington's disease (Zhang, 2019).

While PGC1α's mechanism in other organs or tissues such as muscle and liver are well known, PGC1α in cartilage has not been fully studied yet. Beside its interaction with transcription factors and nuclear receptors associated with mitochondrial respiratory function, PGC1α also binds to SOX9, which is a key transcription factor controlling chondrocyte differentiation and function (Nishimura, 2017). Furthermore, an in vitro study using siRNA showed an increased release of nitric oxide and MMPs (Matrix metalloproteinases) in response to proinflammatory cytokines upon knockdown of PGC1α (Zhao, 2014).

Lastly, a previous study in our lab by Carina Prein has shown that the PGC1α gene is important for maintaining joint health (Prein, in prep.) In their study, cartilage-specific loss of PGC1α in mice results in accelerated OA during aging, along with changes in mitochondrial parameters and gene expression in chondrocytes.

However, we don't know yet specific mechanisms through which PGC1α regulates cartilage homeostasis and function. Therefore, we aim to reveal the underlying mechanisms of PGC1α function in cartilage and in knee joint health. We built on our previous work with RNA-seq of primary chondrocytes treated with and without a pharmacological inhibitor of PGC1α (SR-19282). Further, we designed primers of selected genes identified in RNA-seq results to validate results. Lastly, we conducted mitochondrial experiments including JC-1 and Mito tracker green staining to reveal if SR-19282 affected mitochondria of chondrocytes by inhibiting PGC1α.

Hypothesis and objectives

Based on the existing literature and our previous findings showed that PGC1a is important for mitochondrial biogenesis and dysfunction of mitochondria can cause OA, we hypothesized that PGC1α plays a crucial role in maintaining mitochondrial function in chondrocytes and that its inhibition would lead to mitochondrial dysfunction, contributing to the progression of OA.

The primary objectives of our research were:

1. To investigate the effects of PGC1α inhibition on mitochondrial function in chondrocytes.

2. To analyze the changes in gene expression profiles associated with mitochondrial biogenesis and function following PGC1α inhibition.

3. To explore the potential pathways affected by PGC1α inhibition using RNA sequencing and pathway enrichment analyses.

1.1 Osteoarthritis

OA, one of the most dominant and incapacitating joint disorders, involves articular cartilage damage and results in pain, functional disability, and substantial impact on life quality (Arden & NEVITT, 2006). Knee OA is a form of OA where cartilage degrades, and osteophytes develop while there is also synovial inflammation (Park,2024). This often leads to pain in the knee joint with limited movement. There has been a traditional belief that osteoarthritis originates from the articular cartilage of joints. However, it is now known that the whole joint including surrounding muscles and other joint structures are affected by this condition (Marks, 2017). This disease leads to joint pain, stiffness, and a significant reduction in the quality of life. Despite the prevalence of OA, current treatment options are largely palliative, focusing on pain management and symptom relief rather than addressing the underlying causes (Marks, 2020). This is largely due to the incomplete understanding of the molecular mechanisms driving the disease.

Understanding the mechanisms of OA is a complex challenge due to several interrelated factors, including the multifactorial nature of the disease, the variability in patient presentations, and the limitations of current research methodologies (Stone & Baker, 2015).

Firstly, OA is a multifactorial disease characterized by a combination of genetic, environmental, and lifestyle factors that contribute to its development and progression. The interplay between these factors complicates the identification of specific mechanisms involved in OA (Su, 2022).

Secondly, the heterogeneity of OA presentations adds another layer of complexity. OA can manifest differently across individuals, with variations in symptoms, severity, and affected joints (Shah, 2022).

Moreover, advancements in molecular biology have revealed that OA is not merely a degenerative "wear and tear" condition but rather an inflammatory disease involving complex biochemical pathways (Mobasheri & Levesque, 2019). The involvement of inflammatory mediators, such as cytokines and metalloproteinases, in the pathogenesis of

OA needs a deeper understanding of these mechanisms (Li, 2020). However, effective disease-modifying therapies still remain elusive, indicating that our understanding of mechanisms of OA is still incomplete (Su, 2022).

A. Healthy Knee joint   B. Osteoarthritic knee joint

Bone
Synovial membrane
Articular cartilage
Meniscus
Synovial fluid

Infammation of
the synovial membrane
Subchondral bone
sclerosis
Fibrillated cartilage
Osteophyte
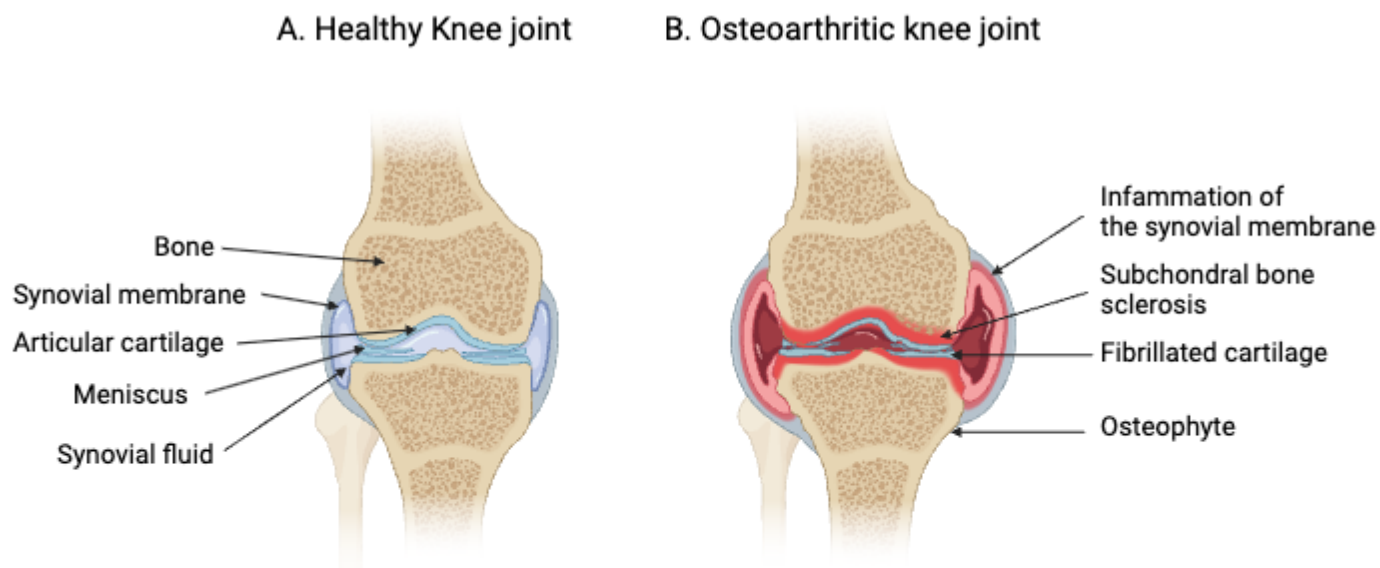
Figure 1.1 Structural comparison of osteoarthritic knee with healthy knee

(A) healthy knee joint with healthy bone, meniscus and articular cartilage. (B) in osteoarthritic knees, osteophytes, bone cysts and sclerosis occur in subchondral bone. Fibrillated cartilage, meniscal tear, and inflammation of synovial membrane are other abnormalities in osteoarthritic knee joints (Sadri, 2021). Figure was generated with Biorender.

1.2 Articular cartilage

Articular cartilage is a specialized connective tissue that covers the surfaces of bones in joints and provides a smooth surface for low friction movement (Othman, 2004). It is a thin heterogeneous tissue made up of collagen, proteoglycan and, water with average thickness less than 2 mm in human (Othman, 2004). Articular cartilage acts as a load bearing tissue in the joints and thus plays an important role in the biomechanics and morphologic properties of the tissue (Zheng, 2010). This tissue is very important because it ensures efficient transmission of loads to subchondral bone, mediating almost frictionless sliding between articular surfaces (Raya, 2015).

The role of articular cartilage's structural architecture is critical for its function as a friction-reducing and load-bearing cushion in the synovial joints (Sandra, 2016). It displays zonal differences in cell distributions and collagen fiber designs, with collagen fibrils being responsible for strengthening during tensile force and proteoglycans, which provide compressive stiffness that permits regular movement (Dodge & Poole, 1989). The structure of collagen fibrils within articular cartilage actually divides the tissue into three consecutive structural layers, which are superficial zone, transitional zone and radial zone, bearing distinct collagen orientations (Zheng & Xia, 2010). Thus, articular cartilage is a multi-layered structure lining the surfaces of all joints characterized by nonlinear, un-uniformity porous-viscoelastic properties (Sandra, 2016). Chondrocytes, collagen fibers, proteoglycans and water make up most of its composition (He, 2014). This implies that the tissue undergoes simultaneous resorption and neoformation during postnatal development which exemplifies its dynamic nature (Hunziker, 2007).

Chondrocytes regulate the microstructure of articular cartilage, which is affected by the mechanical conditions prevailing, thus emphasizing that if we want to have good tissue quality, we have to optimize loading (He, 2013). Changes taking place in the micromechanical properties of articular cartilage and subchondral bone's microstructure have been linked with spontaneous hip osteoarthritis in animals models identifying joint tissues interconnectedness during disease development (Gao, 2023). Moreover, articular cartilage mineralization induced by ATP or other factors may influence tissue integrity and dysfunction through ectopic mineralization and calcification processes (Felisbino &

Carvalho, 2002). Articular cartilage is therefore a complex mix of elements organized that it facilitates soft articulation, transmission of loads, and normality of joints.
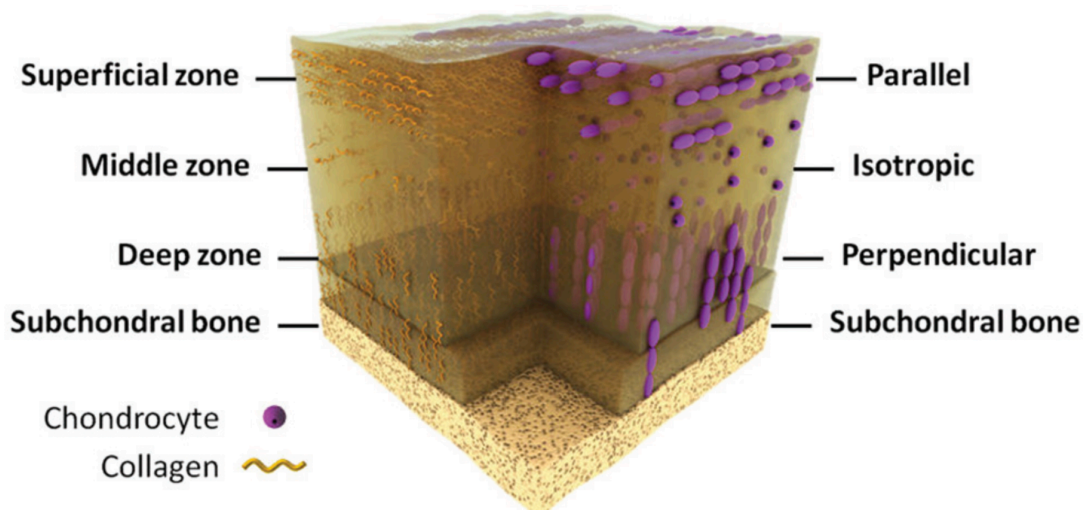
Figure 1.2 Schematic representation of the multi-zonal structure of articular cartilage showing the collagen and cell orientation.

Cartilage varies along the depth of the tissue with respect to the orientation of the constituents, composition of the ECM, as well as by the shape and arrangement of chondrocytes. Chondrocytes in different zones reveal distinct morphologies and express specific markers that are characteristic of each zone. This layered structure is generated upon maturation as a result of applied and generated hydrostatic forces through the tissue and can be divided into the following zones: the top layer, also referred to as a superficial or tangential zone, the middle or transitional zone, the deep or radial zone, and the calcified zone (Figure from Sandra, 2016. Permission reserved).

1.3 Chondrocytes

Articular cartilage cells known as chondrocytes are located within the cartilage matrix and perform a critical duty of maintaining the cartilage's health and function. These cells are responsible for the manufacturing and preservation of the ECM of cartilage (Cancedda, 2009). Chondrocytes play an imperative role in maintaining the equilibrium of cartilage tissue including the synthesis as well as decomposition of the matrix to support proper cartilage functions (Kulyar, 2024).

In a healthy joint, chondrocytes maintain physiological and metabolic balance with strong redox control over differentiation and chondrogenesis (Bai, 2019). A disruption in cartilage homeostasis leads to osteoarthritis. Chondrocytes in osteoarthritic cartilage transition to a hypertrophic phenotype and undergo apoptosis (Zheng, 2021). In the environment of a joint with osteoarthritis and under inflammatory conditions, chondrocytes undergo a metabolic imbalance and cartilage remodeling. This involves increased glycolysis, impaired mitochondrial function, and chondrocyte senescence (Mobasheri, 2017).

Specific to OA, chondrocytes are in the centerpiece of the disease process and play a crucial role in the development of the condition. The early phase of OA is characterized the production of matrix proteins, proteinases, growth factors, cytokines and inflammatory mediators by chondrocytes (Goldring, 2007). These changes in chondrocyte behavior result in the net degradation of cartilage matrix as well as the progression of the disease process in OA. Mechanical damage is considered a significant factor in the development of OA, as chondrocytes react differently to molecular signals depending on their location within the joint. (Goldring & Marcu, 2009).

Chondrocyte release of molecular signals such as cytokines that may alter their anabolic and catabolic activities is sensitive to mechanical forces (Issa, 2012). Any change in the chondrocyte activity such as enhanced apoptosis rates or skewed gene regulation can cause cartilage degradation in a disease such as OA (Rades, 2018).

Chondrocytes are also involved in responding to growth factors, hormones and cytokines, affecting the biosynthetic activity of the cells toward cartilage repair and regeneration (Cornish, 2015). In their immediate microenvironments, chondrocytes must sense and respond to mechanical forces, or mechanosensory signaling; this is facilitated through the cytoskeleton of chondrocytes (Mainil-Varlet, 2012). Also, chondrocytes have other paracrine functions such as regulating inflammation via interleukins, cellular adhesion by integrins and regulation of RNA-binding proteins regulating arthritis and cartilage (McKenna & Aigner, 2002).

Overall, chondrocytes are essential cells in maintaining the health and function of articular cartilage. They have significant interactions with mechanical, molecular, and inflammatory signals that highly contribute to the process of OA and other problems with cartilage. The knowledge of the behavior, as well as the functions of chondrocytes is central in the formulation of therapies and intervention measures to treat conditions like OA.
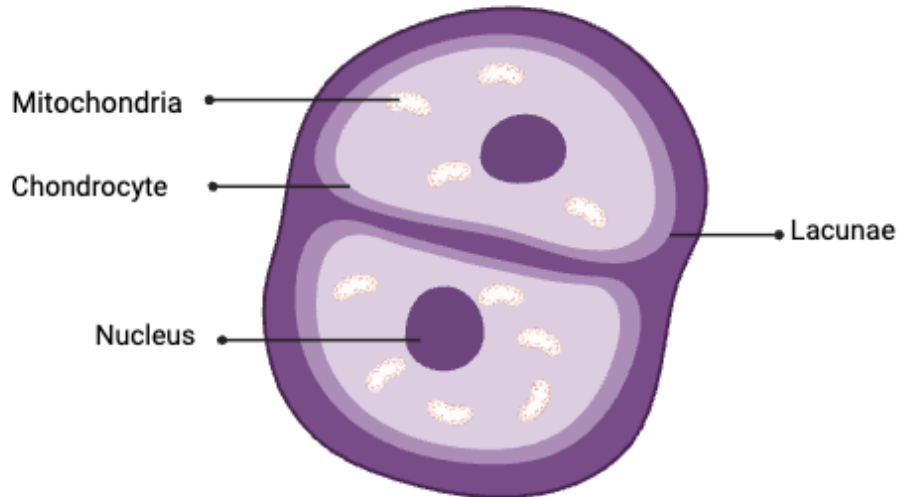
Figure 1.3 The structure of Chondrocyte

Adult chondrocytes exhibit different morphologies in different layers due to their positions within cartilage. Cartilaginous superficial zone chondrocytes usually appear flattened and elliptical, aligned parallel to the surface. Chondrocytes in the mid-zone display a spheroidal shape with a larger size and are arranged randomly, whereas those in the deep zone are predominantly rounded and aligned in perpendicular columns. Mature chondrocytes are mostly distributed in chondrocyte clusters in groups of 2-8. Under the electron microscope, chondrocytes have protrusions and wrinkles, and there are a substantial rough endoplasmic reticulum, a developed Golgi complex, and a small number of mitochondria in the cytoplasm. Chondrocytes are buried in the cartilage interstitium, which is in a small cavity called a cartilage lacuna. Figure was generated with Biorender.

1.3.1 Immature murine articular chondrocyte culture

Immature murine articular chondrocytes or iMACs present an unique cell culture system that is widely used in research to model osteoarthritis and study the mechanisms of cartilage degradation. These chondrocytes are derived from neonatal murine articular cartilage and expanded in culture dishes for the investigation of different facets of OA pathogenesis (Salvat, 2005). Thus, using iMACs, one can study the molecular basis of OA, assess the efficacy of possible treatments, and determine the impact of various factors on the maintenance of cartilage and the development of OA.

The culture of iMACs is useful for understanding the chondrocyte response to stimuli including growth factors, cytokines and mechanical forces in mice model (Eegher, 2021). Culture conditions of iMACs can be modified to reflect the OA microenvironment and determine the alterations in gene expression, protein synthesis and other cellular processes that occur during cartilage degradation (Ratneswaran, 2017). This model enables the study of signaling pathways, gene regulation, and cellular activities implicated in OA development.

Research employing iMACs has shown that it is useful for assessing the impact of numerous factors on chondrocyte differentiation, matrix synthesis and degradation and inflammatory processes associated with OA (Huang, 2016). Primary chondrocyte isolation from human cartilage tissue also undergoes similar protocol as iMACs (Tew, 2008). Thus, understanding the gene expression, metabolic activity and phenotypic characteristics of chondrocytes obtained from OA patients may help elucidate the molecular mechanisms underlying the pathogenesis of the disease and identify novel molecular targets for its treatment (Olivotto, 2013). Moreover, the use of iMACs allows for analyzing epigenetic changes, cell aging, and oxidative stress in the framework of OA formation (Kim, 2023).

Besides, iMACs can be used to study the effects of growth factors, cytokines, and pharmacological agents on chondrocyte function and cartilage health (Pérez-Lozano, 2022). As such, by regulating the culture conditions of iMACs, the response of

chondrocytes to various treatments regarding their metabolism, matrix synthesis, and inflammation in the context of OA can be investigated (Sun & Beier, 2019). This model system is therefore useful in the identification of potential therapeutic agents and the understanding of the processes involved in the development of OA.

Overall, iMAC is a flexible and helpful model to explore osteoarthritis. Thus, the use of iMACs enables the study of the cellular and molecular mechanisms of OA, as well as the discovery of new therapeutic targets, and the elucidation of the process of cartilage degradation in this common joint disease.
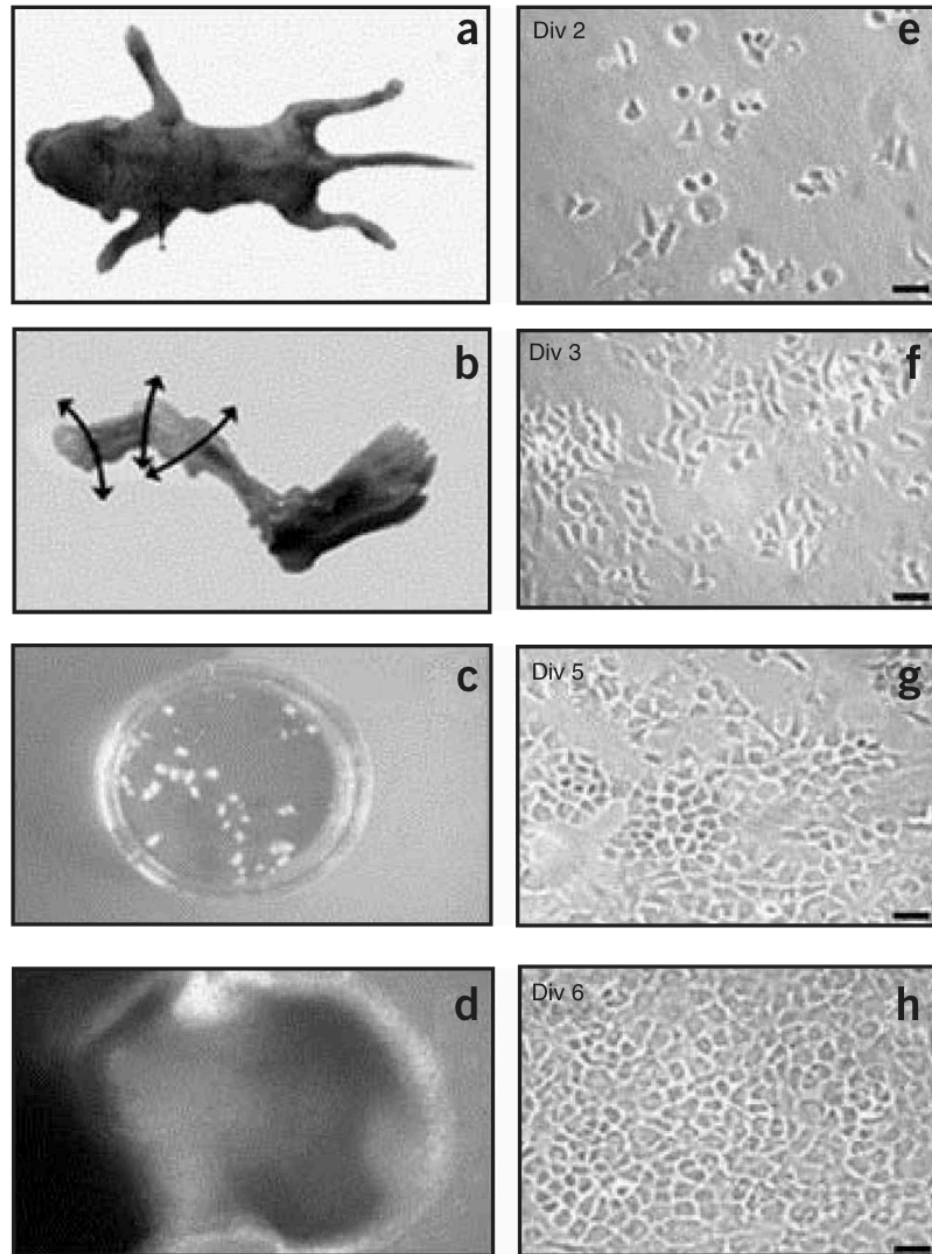
Figure 1.4 Primary culture of immature murine articular chondrocytes

(a) Skin and soft tissues were removed from the hind legs of 5 day-old mice. (b) Soft tissue of the joints was discarded to isolate the femoral heads, condyles, and tibial plateaus. (c) Cartilage pieces were washed and incubated with collagenase D. (c) A cartilage piece after overnight incubation with collagenase D. (e–h) Phase-contrast micrographs of mouse newborn articular chondrocytes plated on culture dishes after 2days, 3days, 5days, and 6ays. (Figure from Gosset, 2008. Permission reserved)

1.4   Mitochondria

1.4.1 Mitochondria's function as cellular organelle.

Mitochondrial biogenesis is the multiplication of pre-existing mitochondria to ensure that there are enough functional organelles in a cell to meet its metabolic needs; it is the process of making new mitochondria. This process is tightly coordinated, and mtDNA and nDNA transcription and translation are coupled, with synthesis synchronized by the OXPHOS complex assembly (Onyango, 2010). Properly balanced mitochondria, with an adequate number of functional units, are indispensable to meet the metabolic needs of the cell and maintain mitochondrial homeostasis (Xu, 2020).

Fission and fusion are critical processes through which mitochondrial quality is ensured and population is regulated. Fission secures the division of one mitochondrion into two organelles, important for removing damaged regions and distributing the mitochondria in cell division (Popov, 2020). As opposed to this, fusion combines two mitochondria and homogenizes the contents of the partially damaged mitochondria, thereby reducing stress upon them.

Mitophagy is defined as the selective removal of damaged mitochondria by the autophagic route; it becomes a critical checkpoint in quality control. In this way, both mitophagy and biogenesis cooperate with each other to set a healthy number of mitochondria in a cell by removing the bad ones. This reciprocal process of mitochondrial biogenesis and mitophagy is very essential within the cells to clear damaged organelles and make new functional mitochondria. The major function of the mitochondria is the generation of adenosine triphosphate, which results from oxidative phosphorylation in the electron transport chain. A protein chain translocates these electrons down these ETC for ATP formation (Shao, 2021).

The mitochondria also undertake a process known as beta oxidation, the process by which fatty acids are broken down to form acetyl-CoA, which in turn enters the citric acid cycle to produce ATP. This is hugely important, particularly to tissues that require high energy outputs; it is mainly the most abundant source of fuel to the heart and

skeletal muscles—tissues using fatty acids as their energy source. They further maintain the cell's redox state and regulate the levels of oxidative stress. They catalyze redox reactions, with ROS define made as a byproduct of the oxidative phosphorylation process. The ROS play various roles in cell signaling and homeostasis. Apart from the molecular ROS, mitochondria have independent defense antioxidants to eradicate unnecessary ROS that could be destructive to the cell (Andrés, 2014).

Mitochondria play a significant role in apoptosis, which is a programmed mechanism of cell death. They initiate the intrinsic apoptotic pathway by the release of cytochrome c. This release in turn triggers caspase activation as well as the execution of cell death. This role is for clearing out unhealthy or unwanted cells hence preserving the balance of the tissues and avoiding diseases like cancer (Dong, 2015).

Mitophagy and mitochondrial biogenesis are known to be associated with different diseases these include neurodegenerative diseases and aging. For example, in Alzheimer's disease, the decrease in the rate of mitochondrial biogenesis is a potential factor in the development of the untoward disease, through an influence on cellular energy levels and the increase in oxidative stress (Zhu, 2021). Likewise, in other age-related pathologies, adequate mitochondrial positioning in the cytoplasm and their biogenesis is critical for cell vitality (Bernard, 2017).

Mitochondrial biogenesis is also significant for the cellular reaction to external factors, including exercise. Exercise leads to the creation of new mitochondria to cater for the higher energy requirements hence improving metabolic potential and function of cells (Lee, 2022). This flexible response further emphasizes the significance of mitochondrial dynamics in mediating variations in physiology and cellular energy state.

Overall, mitochondria are complex structures that play an important role in cell metabolism, regulation of redox potential, and apoptosis. Biogenesis, fission/fusion, and mitophagy regulate the quality of mitochondria population and the overall network. Knowledge of these regulatory mechanisms is crucial when seeking to find a way on how

to treat diseases that are characterized by mitochondrial dysfunction. Thus, mitochondria can argue the balance of cellular processes and providing the cells with energy that is necessary for their proper functioning.

1.4.2 Structure of mitochondria in chondrocyte

Mitochondrial structure is formed by the existence of two distinct membranes, the outer membrane, and the inner membrane. The outer membrane is the border that encloses the mitochondrion and separates it from the cytosol. On the other hand, the inner membrane encloses the mitochondrial matrix, which has significant folding that forms cristae. These cristae increase the surface area of the inner membrane for space, which houses all the central processes like oxidative phosphorylation and ATP production by the mitochondria (Wang, 2024).

The inner mitochondrial membrane harbors an electron transport system bearing all the functions in the generation of ATP through aerobic phosphorylation. It bears the major components of the electron transport chain, like the complexes of the electron transfer chain, and ATP synthesis in its composition. Disruptions of this kind of structure could have detrimental impacts on the efficiency of the electron transport system, resulting in low ATP production and possible cell dysfunction (Wang, 2024).

On the other hand, the outer membrane of mitochondria is involved in such functions as protein import regulation and the maintenance of mitochondrial dynamics. Proteins like Bcl-2 interact with the outer membrane, thereby controlling processes like apoptosis and maintaining mitochondrial integrity (Epand, 2003). The outer membrane also provides a vital interface through which mitochondria interact with the cytosol to enable some molecules to be exchanged from within or outside the cell through this organelle (Yamashita, 2016).

1.4.3 Importance of mitochondria in knee joint health

Mitochondria are involved in the regulation of the knee joint through several processes that have an influence on the joint's structure and functionality. Mitochondria are vital structures that are involved in the generation of energy especially in tissues that require high energy input such as the knee joint which experiences constant mechanical stress and movement (Blanco, 2004). Malfunction of mitochondria is associated with osteoarthritis, which shows the importance of these organelles in the maintenance of joints (Blanco, 2004). Cartilage, ligaments, synovium, all the tissues implicated in the knee joint are metabolically active, and their repair and maintenance involve energy expenditure, thus the need for mitochondria in maintaining knee joint function.

In addition, the nerves linking the knee joint with the lumbar spinal cord and other significant parts of the body require healthy mitochondria to support nerve impulses and preserve the network that is crucial for the knee joint's functionality (Marks, 2022). This study discusses how mitochondrial functioning and neural networks are interconnected in the regulation of movement, sensory input, and knee joint health. Abnormalities in these mitochondrial pathways can affect the neural pathways and consequently the knee joint health and functionality (Marks, 2022; Kan, 2021).

Neuro-mechanical movements are influenced by mitochondria since they are involved in controlling movement efficiency and joint health that can prevent osteoarthritis (Seeley, 2022). Appropriate biomechanics and joint kinematics are necessary to decrease the load on the knee joint and avoid injuries or deterioration of the joint. Muscles which participate in the movements of the knee joint require energy and mitochondria are involved in this process thus affecting the biomechanics of the knee joint and its longevity (Heijink, 2012).

Mitochondrial health is associated with cartilage health in the knee joint, which is vital in the prevention of diseases such as osteoarthritis (Madhu, 2024). It has been revealed that proteins such as OPA1 are involved in maintaining the structure and metabolic processes of mitochondria and thus protecting the health of the cartilage in the knee joint (Madhu, 2024). Thus, mitochondria are involved in energy metabolism of chondrocytes – the cells

that are the main components of cartilage, thus stressing the role of mitochondria in maintaining the integrity of the knee joint.

Moreover, mechanical stress, which is a consequence of biomechanical factors and changes in movement patterns, has been linked to the development and further progression of knee osteoarthritis (Wasser, 2023). They are involved in the regulation for adapting to changes in joint loading and supplying metabolic needs of the tissue within the knee joint thus affecting the onset of osteoarthritis. Mitochondrial dysfunction leads to imbalances of energy availability and utilization in the knee joint, which is detrimental to the joint's health and can cause degenerative changes (Kan, 2021).

In conclusion, mitochondria have a complex function of contributing to the function of knee joint through energy production, neural signaling, biomechanical forces, cartilage health, and adaptation to biomechanical forces. The complex dependency of the knee joint on mitochondrial function and the many aspects of the joint's physiology highlights the significance of these organelle for the proper functioning and overall health of the knee joint. Thus, understanding specific mechanism of dysfunction of mitochondria and how this affects cartilage health is essential to investigate new therapeutic methodology of OA.
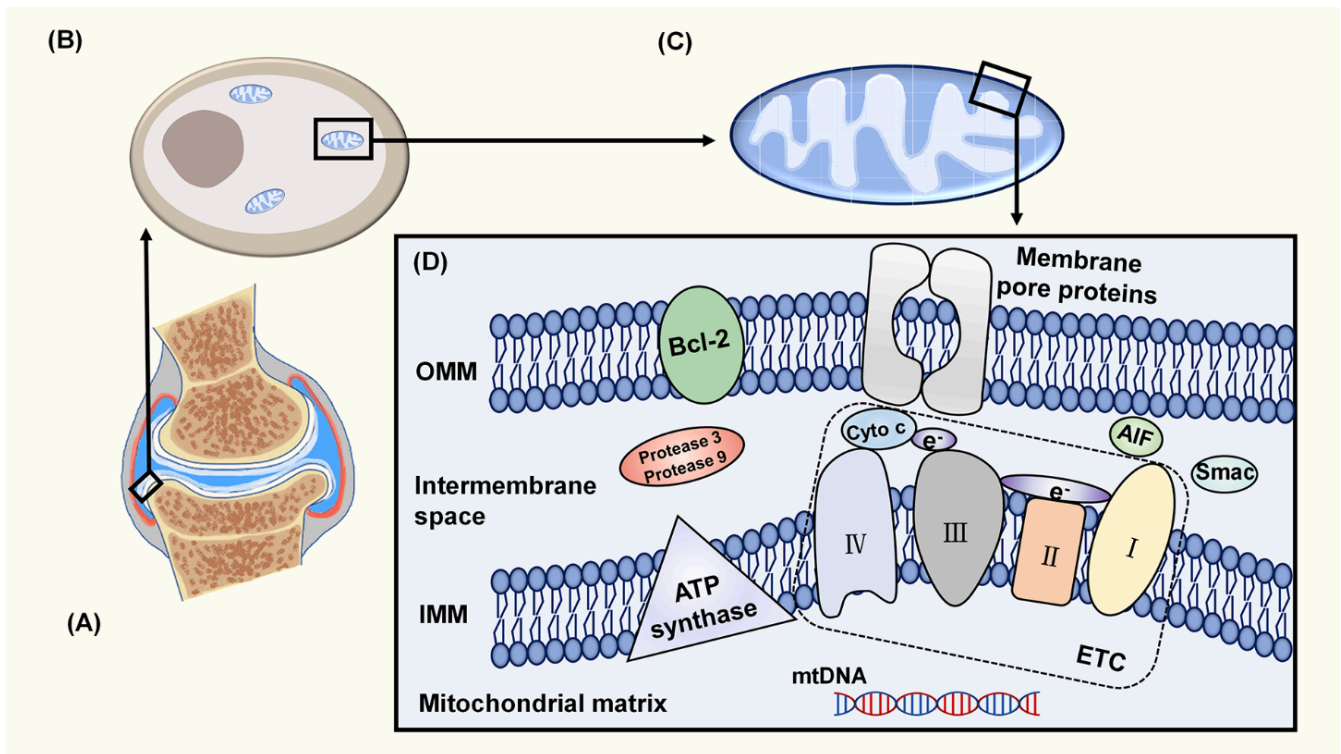
Figure 1.5 Mitochondrial structure in Chondrocyte

(A) Articular cartilage structure. Articular cartilage is composed of ECM and chondrocytes. ECM is mainly composed of type-2-collagen and aggrecans. (B) Chondrocyte structure from articular cartilage. Chondrocytes have distributed mitochondria in cytoplasm. (C) Mitochondria diagram (D) Mitochondrial outer membrane and inner membrane structure. IMM has electron transport system and ATP synthase, and OMM has Bcl-2 and membrane pore proteins. Other functional proteins are located in intermembrane space. (Figure from Kan, 2021. Permission reserved)

1.5 Peroxisome proliferator-activated receptor-gamma coactivator (PGC)-1alpha

The PGC1α gene, which is peroxisome proliferator-activated receptor gamma coactivator 1-alpha, is critical to the mitochondria. PGC1α is a transcriptional coactivator involved in the regulation of genes that are involved in mtDNA (mitochondrial DNA) synthesis, oxidative phosphorylation and energy expenditure (Austin & St-Pierre, 2012). It binds and communicates with other proteins, e.g. transcription factors and nuclear hormone receptors, to control the processes of genes responsible for mitochondrial processes and cell energy metabolism.

PGC1α is also involved in the regulation of genes that are involved in the process of mitochondrial biogenesis such as *Tfam* and *Nrf1* (Austin & St-Pierre, 2012). This mutual regulation of gene expression is critical in sustaining the structure and function of the organelle.

PGC-1α plays a functional role in endurance exercise-induced mitochondrial biogenesis and angiogenesis, but not IIb-to-IIa fiber-type transformation in mouse skeletal muscle (Geng, 2010). PGC1α is highly expressed in oxidative tissues such as heart, muscle, kidney, and brain (Rius-Pérez, 2020). It is a positive regulator of mitochondrial biogenesis and respiration. Altered expression or activity of PGC1α has been reported in several disorders associated with oxidative stress, including Parkinson's disease, Alzheimer's disease, and Huntington's disease (Yang, 2023).

In addition, PGC1α is reported to mediate thermogenic gene expression upon cold exposure and beta-adrenergic agonists involved in the regulation of energy expenditure and heat generation in brown adipose tissue (BAT) (Osorio-Conles, 2022). It binds to peroxisome proliferator-activated receptor alpha (PPARα) for coactivation of target genes involved in the process of mitochondrial fatty acid oxidation to increase metabolic plasticity and energy expenditure in response to physiological signals (Osorio-Conles, 2022).

1.5.1 Role of PGC1α in Mitochondria

PGC1α is known as a master regulator of mitochondrial biogenesis and oxidative metabolism, playing a critical role in cellular energy production, mitochondrial function, and metabolic homeostasis. PGC1α as a transcriptional coactivator enables the expression of genes involved in mitochondrial biogenesis, oxidative phosphorylation, and thermogenesis, making it a key player in cellular energy metabolism and mitochondrial health (Villena, 2015).

Mitochondrial biogenesis is initiated by an energetic imbalance sensed by wo pathways: AMPK (AMP-activated protein kinase) and SIRT1. Increased expression or activity of the key regulator of mitochondrial biogenesis PGC1α activates the expression of *Nrf-1/2*, which induces the expression of *Tfam*, which translocases to mitochondria, binds to mtDNA, and activates transcription and replication. An increase in OXPHOS proteins reduces ROS generation in mitochondria. Mitochondrial fusion and fission dynamics are also affected by ROS. Dysfunctional mitochondria can be eliminated through a process known as mitophagy (Abu, 2023).

PGC1α influence expression of the genes that are crucial to mitochondrial biogenesis such as mitochondrial transcription factor A (Tfam), nuclear respiratory factor 1 (Nrf1), and Estrogen related receptor alpha (Esrra) (Singh, 2018).

Especially, the interaction between PGC1α and *Esrra* is critical in regulating gene expression and cellular functions related to mitochondrial biogenesis, energy metabolism, and other physiological processes. PGC1α induces mRNA expression of *Esrra* and interacts with *Esrra* to form a heterodimer that mediates transcriptional activity of *Esrra* on target genes (Singh, 2018). The fact that PGC1α is necessary to promote *Esrra* mRNA expression, emphasizes the importance of this interaction in gene regulation and mitochondrial function (Malik, 2023).

PGC1α also coactivates *Tfam* through promoter binding, which leads to the activation of genes that are involved in mitochondrial biogenesis and the regulation of mitochondrial DNA replication (Liang, 2006). Also, VEGFR2 inhibition amplified mitochondrial

biogenesis by decreasing the phosphorylation of PGC1α, which will cause translocation of PGC1α into the nucleus, and increase *Tfam* expression. Therefore, PGC1α subsequently enhances mitochondrial biogenesis (Guo, 2024).

Additionally, PGC1α works as a coactivator of *Nrf1* to transcribe genes that are involved in the replication of mitochondrial DNA and the control of mitochondrial gene expression (Austin & St-Pierre, 2012).
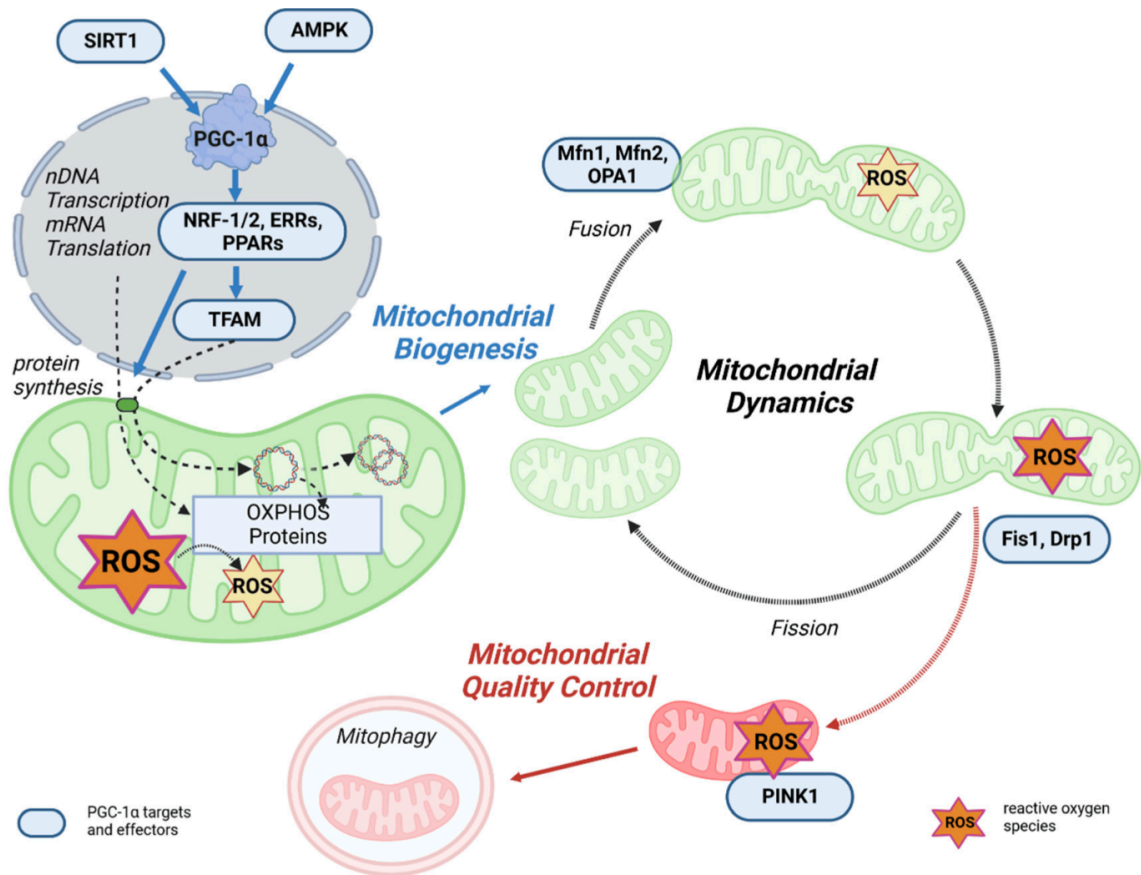
Figure 1.6 Role of PGC1α in mitochondrial biogenesis

AMPK and SIRT1 sensed energetic imbalance and it induce initiation of mitochondrial biogenesis. PGC-1α activates the expression of Nrf-1/2, which induces the expression of Tfam, which translocate to mitochondria, binds to mtDNA, and activates transcription and replication. An increase in OXPHOS proteins reduces ROS generation in mitochondria. Mitochondrial fusion and fission dynamics are also affected by ROS. Dysfunctional mitochondria can be eliminated through a process known as mitophagy. (Figure from Abu, 2023. Permission reserved)

1.5.2 PGC1α Inhibitor

SR-18292 is a small molecule that has shown promising effects in various biological contexts. It has been identified as an inhibitor of PGC-1α (Xie, 2021). SR-18292 inhibits PGC1α through a specific mechanism involving the modulation of PGC-1α acetylation and its interaction with other proteins. SR-18292 increases PGC-1α lysine acetylation, which leads to the inhibition of PGC-1α activity by blocking its interaction with HNF4A (Varuzhanyan, 2024). This interaction blockade is crucial for the inhibitory effect of SR-18292 on PGC1α.

Additionally, inhibiting PGC-1α by SR-18292 has the effect of decreasing the activity of gluconeogenic genes and decreasing the amount of glucose generated by hepatocytes (Yang, 2023). This inhibition is a result of the enhancement of PGC1α acetylation which decreases the coactivation of HNF4A and the stimulation of gluconeogenic genes (Sharabi, 2017).

Moreover, SR-18292 has been implicated in various cellular processes. It has been used to inhibit PGC-1α in studies related to sepsis-induced brain injury. The injection of SR-18292 decreased mitochondrial function (MMP, ATP level, complex I activity), PGC-1a activation, and expression of *Nrf2* and *Tfam* (Xie, 2021). Additionally, SR-18292 has been investigated in the context of neuroprotection, where its inhibition of PGC-1α was found to impact mitochondrial function (Han & Dong, 2020). Furthermore, SR-18292 has been used to evaluate the role of PGC1α in protective effects against gentamicin-induced ototoxicity (Praharaj, 2024). Overall, SR-18292 emerges as a versatile compound with significant implications across various fields of research due to its ability to inhibit PGC1α which results in decreased mitochondrial function.

However, PGC1α is part of a family of coactivators, which also includes PGC1β (PPARGC1B) and PRC (PPARGC1C). These coactivators share some functional similarities but also have unique roles in cellular energy metabolism and other processes (Lin, 2005). If the lysine domain of PGC1α acetylated by SR-18292 is shared domain with PGC1β or PRC, there is a potential cross reactivity. Although studies with SR-18292 only mentioned influence on PGC1α only, experimental data such as binding

assays, in vitro inhibition studies, and gene expression analyses after treatment in cell lines or animal models are needed.

a

b
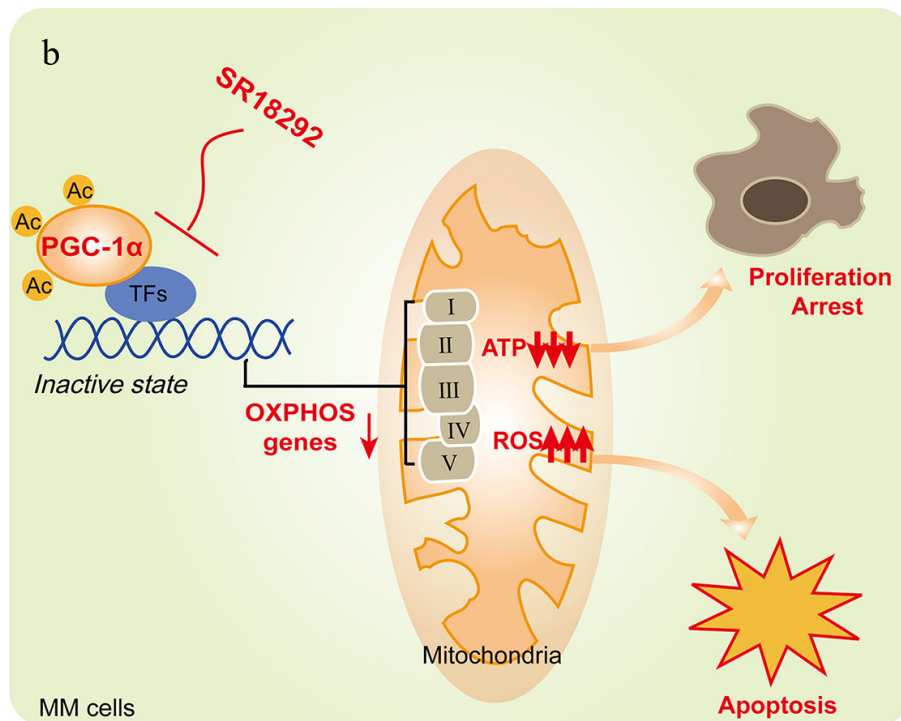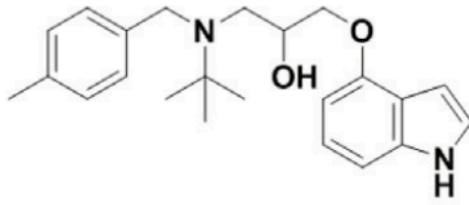
Figure 1.7 SR-18292

(a) Chemical structure of SR-18292 (Sharabi, 2017) (b) Diagram of how SR-18292 affects mitochondrial metabolism. SR-18292 inhibits PGC1α through acetylation which results significantly impaired the proliferation and survival of Murtiple Myeloma cells due to OXPHOS metabolism dysfunction, which leads to energy exhaustion and oxidative damage (Figure from Xiang, 2020. Permission reserved).

Chapter 2

2 Materials and Methods

2.1 Animals in use

All mouse experiments were done in compliance with the Institutional Animal Care and Use Committee guidelines at the London Regional Cancer Center and at Western University (Mouse Protocol Number: 2023-057). CD-1 mice from Charles River that were timed pregnant were used to get neonatal P5 mice for tissue collection. All pregnant CD-1 mice were housed in a temperature- and humidity-controlled room (20-25 °C, 40-60% humidity).

2.2 Immortalized Mouse Articular Chondrocytes (IMACs) culture

P5 neonatal mice were sacrificed and dissected to isolate femoral heads, femoral condyles, and tibial plateau from both right and left legs. Isolated tissues were subjected to 1-hour incubations at 37°C, 5% CO_2 with collagenase D (3mg/ml in Dulbecco's Modified Eagle Medium (DMEM) supplemented with 10% fetal bovine serum (FBS), 1% penicillin-streptomycin (100 U/mL penicillin and 100 µg/mL streptomycin), and 1% L-glutamine (2 mM). Tissue fragments were agitated until all soft tissues detached from the cartilage, and then incubated with collagenase D solution (0.5 mg/ml) overnight at 37°C. Aggregates of digested cartilage from day1 were dispersed by passing the digestion solution sequentially through 25ml, 10ml, 5ml and 2ml pipets. Cells were centrifuged for 10 min at 400xg (RT). Collected chondrocytes were washed with PBS, resuspended in culture medium (DMEM with supplements mentioned above) and counted with hemocytometer. 2×10^4 cells were plated per well in 6 well plate. IMACs reached confluence by day 6-7. Each litter represented one biological replicate.

2.3 SR-18292 use

When IMACs reached confluence by day 7, SR-18292 (Cayman chemical) was treated in three different concentrations as recommended from manufacturer. Three experimental group was treated with 5μM, 10μM, and 20μM respectively. DMSO was treated into control group IMACs since SR-18292 was dissolved in DMSO. SR-18292 should first be dissolved in DMSO and then diluted with the aqueous buffer of choice for maximum solubility according to manufacturer's instruction. We made 1mM, 2mM and 4mM stock solution of SR-18292 with DMSO and dilute them into final concentration with media.

2.4 Quantitative real-time PCR (qPCR)

IMACs were treated with SR-18292 at P7 for 0 hour, 6 hour, 24 hour, and 72 hour for treatment groups. Vehicle group was treated with DMSO. Total RNA was extracted using the TRIzol Reagent (Invitrogen) according to manufacturer's instructions. The concentration and purity of RNA were determined using a NanoDrop ND-2000 spectrophotometer (Thermo Scientific).

First-strand cDNA was synthesized from 1 μg of total RNA using the iScript cDNA Synthesis Kit (Bio-Rad) following the manufacturer's protocol. The reaction mixture included 4 μL of 5x iScript Reaction Mix, 1 μL of iScript Reverse Transcriptase, RNA template, and nuclease-free water to a final volume of 20 μL. The reverse transcription reaction was performed in a thermal cycler (Bio-Rad) with the following program: 5 min at 25°C, 20 min at 46°C, and 1 min at 95°C.

qPCR was performed using the SsoFast EvaGreen Supermix 500 Rxn (Bio-Rad) on a CFX96 Real-Time PCR Detection System (Bio-Rad). Each 20 μL reaction contained 5 μL of 2x SsoFast EvaGreen Supermix, 0.1 μL of each forward and reverse primer (50 μM), 0.5 μL of cDNA template, and 4.4 μL of nuclease-free water. The thermal cycling conditions were 95°C for 3 min, followed by 40 cycles of 95°C for 10 sec and 60°C for 30 sec. A melt curve analysis was conducted to verify the specificity of the PCR products: 95°C for 10 sec, 65°C to 95°C with an increment of 0.5°C every 5 sec. Primers

for targeted genes and Beta-actin as reference gene were from Sigma and their sequences are shown in Table 2.1.

Table 2.1 qPCR primer sequences

Primer Name	Sequence
Actb-For	AGATCAAGATCATTGCTCCTCCT
Actb-Rev	AGGGTGTAAAACGCAGCTCA
Esrra-For	CGAGCCTCTCTACATCAAGGC
Esrra-Rev	CTCCTTGTGCCCTGGAAGG
MPC1-For	GCAAGGACTTCCGGGACTATC
MPC1-Rev	CAGAAGTGCATCTACCGTGGG
Nrf1-For	CTGCAGGTCCTGTGGGAAT
Nrf1-Rev	ATGAGGCCGTTTCCGTTTCT
Tfam-For	GGCCCTTCGCAGACAGTTT
Tfam-Rev	GGCTTATAGGGACCCAGTGA

2.5   RNA extraction and Purification for RNA-seq

IMACs were treated with 5 µM SR-18292 at P7 for 0 hour, 6 hour, 24 hour, and 72 hour for treatment groups. Vehicle group was treated with DMSO. Total RNA was extracted using the TRIzol Reagent (Invitrogen) according to manufacturer's protocol. The concentration and purity of RNA were determined using a NanoDrop ND-2000 spectrophotometer (Thermo Scientific).

Isolated RNA was purified using Monarch RNA Cleanup Kit according to manufacturer's protocol. High quality total RNA (minimum 11 µL 100ng/ µL, 260/280 ratio >1.8) were selected for RNA-seq.

2.6   Bulk RNA-sequencing

Four selected trials (8 samples in total including inhibitor treated and control groups) were sent to London Regional Genomics Centre for sequencing. The quality of RNA were assessed using the p to assure size distribution. They performed ribosomal RNA reduction and created indexed libraries that were sequenced on the Illumina NextSeq using High Output 75 cycle sequencing kit (NextSeq). Bioanalyzer result is shown in figure 2.1. RNA-seq data were processed using the DESeq2 package to identify differentially expressed genes (DEGs) between the experimental and control groups. Genes with an adjusted p-value < 0.05 and a fold change > 1.5 were considered significantly differentially expressed.

2.5.1 KEGG Pathway Analysis

The list of DEGs was input into the KEGG Mapper tool to assign each gene to corresponding KEGG pathways. Gene identifiers were converted to KEGG orthology (KO) terms using the DAVID bioinformatics resource. Enrichment analysis was performed using the ClusterProfiler package in R (version 4.0.5). Pathways with an

adjusted p-value < 0.05 were considered significantly enriched. Enriched pathways were visualized in scatter plot using ggplot2 package in R (version 4.0.5).

2.5.2 Gene Ontology (GO) Analysis

The list of DEGs was annotated with GO terms using the biomaRt package in R (version 4.0.5), which interfaces with the Ensembl database to retrieve GO annotations for each gene. Enrichment analysis was conducted using Metascape. GO terms with an adjusted p-value < 0.05 were considered significantly enriched. To show the top enriched GO terms, bar plot was used.
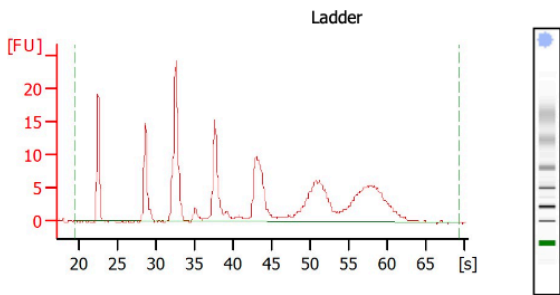
Ladder

Overall Results for Ladder

RNA Area:	231.4
RNA Concentration:	150 ng/µl
Result Flagging Color:	
Result Flagging Label:	All Other Samples

IMACT_1C

Overall Results for sample 1 :   IMACT_1C

RNA Area:	456.6
RNA Concentration:	296 ng/µl
rRNA Ratio [28s / 18s]:	3.0
RNA Integrity Number (RIN):	9.7 (B.02.11)
Result Flagging Color:	
Result Flagging Label:	RIN: 9.70

Fragment table for sample 1 :   IMACT_1C

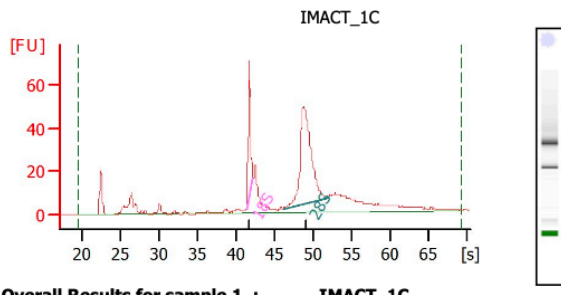| Name	Start Time [s]	End Time [s]	Area	% of total Area
18S	41.43	42.24	49.8	10.9
28S	46.10	51.83	149.3	32.7
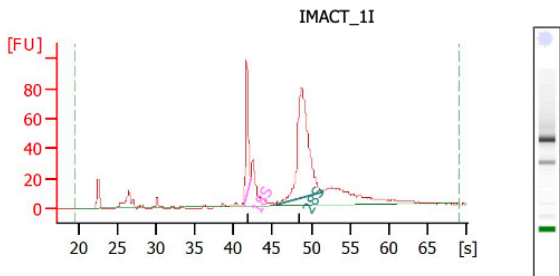
IMACT_1I

Overall Results for sample 2 :   IMACT_1I

RNA Area:	649.2
RNA Concentration:	421 ng/µl
rRNA Ratio [28s / 18s]:	3.3
RNA Integrity Number (RIN):	9.7 (B.02.11)
Result Flagging Color:	
Result Flagging Label:	RIN: 9.70

Fragment table for sample 2 :   IMACT_1I

Name	Start Time [s]	End Time [s]	Area	% of total Area
18S	41.34	42.19	73.4	11.3
28S	45.35	51.46	241.8	37.3
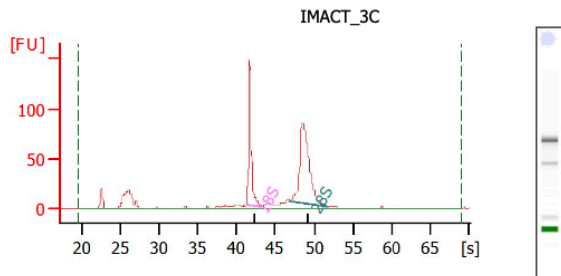
IMACT_3C

Overall Results for sample 3 :   IMACT_3C

RNA Area:	578.5
RNA Concentration:	375 ng/µl
rRNA Ratio [28s / 18s]:	1.7
RNA Integrity Number (RIN):	9.8 (B.02.11)
Result Flagging Color:	
Result Flagging Label:	RIN: 9.80

Fragment table for sample 3 :   IMACT_3C

Name	Start Time [s]	End Time [s]	Area	% of total Area
18S	41.34	43.35	138.1	23.9
28S	46.85	51.87	234.7	40.6
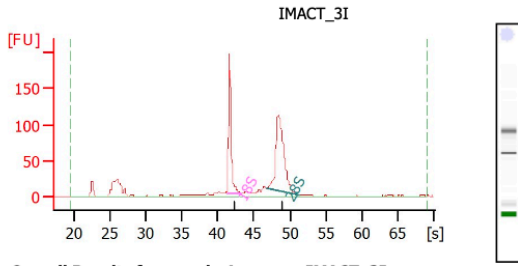
IMACT_3I

Overall Results for sample 4 :   IMACT_3I

RNA Area:	797.9
RNA Concentration:	517 ng/µl
rRNA Ratio [28s / 18s]:	1.6
RNA Integrity Number (RIN):	9.6 (B.02.11)
Result Flagging Color:	
Result Flagging Label:	RIN: 9.60

Fragment table for sample 4 :   IMACT_3I

Name	Start Time [s]	End Time [s]	Area	% of total Area
18S	41.29	43.35	178.6	22.4
28S	46.75	51.36	292.7	36.7
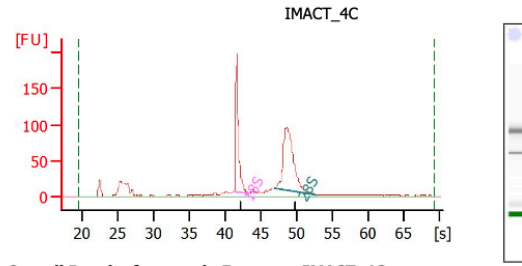
IMACT_4C

Overall Results for sample 5 :   IMACT_4C

RNA Area:	903.3
RNA Concentration:	586 ng/µl
rRNA Ratio [28s / 18s]:	1.6
RNA Integrity Number (RIN):	9.6 (B.02.11)
Result Flagging Color:	
Result Flagging Label:	RIN: 9.60

Fragment table for sample 5 :   IMACT_4C

Name	Start Time [s]	End Time [s]	Area	% of total Area
18S	41.28	43.24	197.9	21.9
28S	46.86	52.83	308.2	34.1
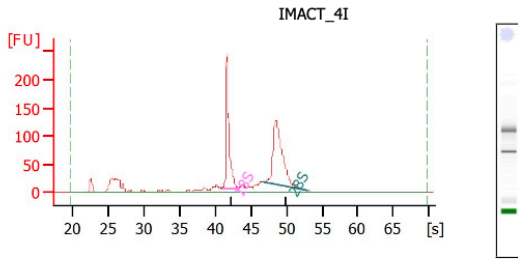
IMACT_4I

Overall Results for sample 6 :   IMACT_4I

RNA Area:	1,217.7
RNA Concentration:	789 ng/µl
rRNA Ratio [28s / 18s]:	1.3
RNA Integrity Number (RIN):	9.4 (B.02.11)
Result Flagging Color:	
Result Flagging Label:	RIN: 9.40

Fragment table for sample 6 :   IMACT_4I

Name	Start Time [s]	End Time [s]	Area	% of total Area
18S	40.90	43.38	282.5	23.2
28S	46.72	53.04	362.8	29.8
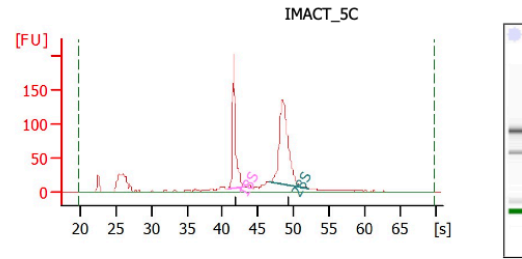
IMACT_5C

Overall Results for sample 7 :   IMACT_5C

RNA Area:	1,072.2
RNA Concentration:	695 ng/µl
rRNA Ratio [28s / 18s]:	1.6
RNA Integrity Number (RIN):	9.6 (B.02.11)
Result Flagging Color:	
Result Flagging Label:	RIN: 9.60

Fragment table for sample 7 :   IMACT_5C

Name	Start Time [s]	End Time [s]	Area	% of total Area
18S	40.79	43.12	232.1	21.6
28S	46.67	52.20	374.3	34.9
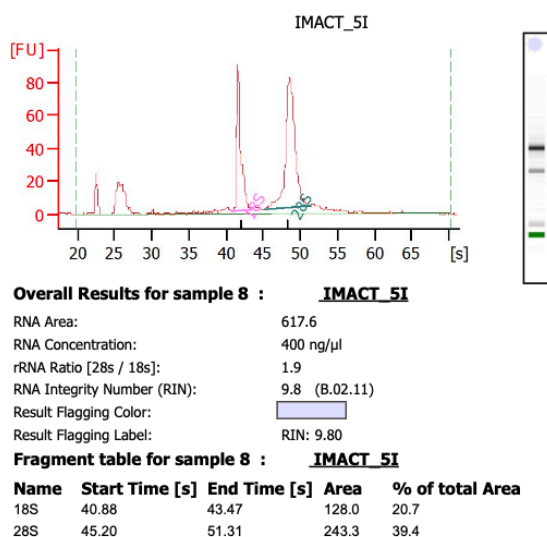
Figure 2.1 Electropherogram summary of RNA samples for RNA-seq

Electropherogram is a visual representation of the results obtained from electrophoresis, where DNA, RNA, or protein samples are separated. Performing electropherogram before RNA-seq allows to get RNA quality assessment, quantification of RNA, RNA profiling and verification of rRNA removal. All 8 samples (4 controls and 4 treatment groups) showed enough quality and quantity to perform RNA-seq. Agilent 2100 Bioanalyzer was used to generate electropherograms.

2.7   Primer design and verification

Primers were designed used for quantification of *Pouf2f2, Slc22a3, Pmaip1, Cxcl13, Slc22a3* and *Sp110* mRNA expression under use of PGC1-alpha inhibitor. Selected gene's mRNA/Genomic alignments FASTA format was obtained using UCSC Genome Browser. They were further analyzed using NCBI Primer Blast to ensure amplicon length fell between 65-150 nucleotides, primers had GC content between 40 and 60% to increase binding stability and had a predicted melting temperature between 58°C and 68°C. Primer sequences are in table 2.2. *Actb* was selected as the reference gene. Optimization of designed primers was performed with a standard PCR reaction using 2× GoTaq Green Master Mix (Promega). Duplicated series were prepared for each PCR reaction to run a strip at both 58°C and 60°C for annealing temperature. *Pla2g4b* was excluded from further experiment by showing visible off-target binding or primer dimers. *Pouf2f2, Slc22a3, Sp110, Cxcl13*, and *Pmaip1* primer pairs didn't have visible off-target binding or primer dimers and had an optimal annealing temperature of 60°C. The efficiency and specificity of these primers were tested with a standard curve.

cDNA was diluted in a series of 2-fold serial dilutions and used in PCR reactions with primers to build standard curves for each primer set. Each sample was loaded in triplicate. 2× GoTaq Green Supermix (Promega) was used for efficiency testing of qPCR primers at 300nM. The PCR reaction ran for 40 cycles with an annealing temperature of 60°C using the Bio-Rad CFX384. Efficiency, R2 values and Ct values for melt curves were calculated using BioRad CFX Manager Software and evaluated prior to running experimental qPCRs. The efficiency is between 90-110% for reliable quantification.

Table 2.2 Designed qPCR primer sequences

Primer Name	Sequence
Actb-For	AGATCAAGATCATTGCTCCTCCT
Actb-Rev	AGGGTGTAAAACGCAGCTCA
Cxcl13-For	ATCGGATTCAAGTTACGCCCC
Cxcl13-Rev	CCATTTGGCACGAGGATTCA
Pmaip1-For	GCACCGGACATAACTGTGGT
Pmaip1-Rev	GGAGTTGAGCACACTCGTCC
Pou2f2-For	CAGCACCAAGATCAAGGCTGAAG
Pou2f2-Rev	GCTGGAGGAGTTGCTGTATGTC
Slc22a3-For	CGTTTCTGCTCTTTCGGCTG
Slc22a3-Rev	GCAATGCCCTTCGTTTCAGG

2.8   Fluorescence Imaging

Same IMACs protocol (methods 2.2) were used to obtain chondrocytes. Cells were treated with 5 µM SR-18292 for 0 hour (control), 6 hour, 24 hour, and 72 hour. At P7, cells were washed twice with PBS and harvested using cell scraper and 2×10^5 cells per well were seeded on a 96-well black bottom plate (Thermo Scientific) triplicate for each group. Cells were allowed to attach for two nights. After staining with JC-1 (Abcam) and MitoTracker Green dye (Invitrogen), plates were imaged using Leica fluorescence microscope. For JC-1 fluorescence imaging, expose to RFP for 0.5 sec, GFP for 2 sec was enough to get signal. 3 sec of exposure was enough for MitotTracker Green imaging. Three images were obtained from each well and cells were randomly picked among the ones who were not overlapped with other cells for clear image.

2.7.1 JC-1 staining

The JC-1 Mitochondrial Membrane Potential Assay Kit (Abcam) was used for JC-1 staining according to manufacturer's protocol. 100 µl/well of 30 µM JC-1 was added for 10 min at 37°C and gently washed with PBS twice before imaging.

2.7.2 MitoTracker Green staining

The MitoTracker Green FM kit (Invitrogen) were used for MitoTracker Green staining. Preparation of MitoTracker Green FM probes was following manufacturer's protocol. 150 nM MitoTracker Green FM probes was used for 30 mins at 37°C and gently washed with PBS twice before imaging.

2.9 Statistical Analysis

2.8.1 Quantitative PCR

The threshold cycle (Ct) values were obtained using the CFX384 Manager Software (Bio-Rad). Relative gene expression levels were calculated using the $2^{-\Delta\Delta Ct}$ method. *Actb* was used as the reference gene for normalization. Each sample was run in triplicate, and the mean Ct value was used for analysis. Statistical analysis was performed using GraphPad Prism 9 software. Differences between groups were analyzed using an Kruskal Wallis test with multiple comparisons, and p-values < 0.05 were considered statistically significant. Relative normalized expression, the quantity of *Actb* transcript in the control group was set to 1, the level of other gene transcripts in the control groups demonstrating changes in transcript expression between inhibitor treated groups and control. The relative expression of the transcripts was normalized to the reference gene (*Actb*) and plotted.

2.8.2 RNA-seq

STAR was used to read alignment and map RNA-seq reads to a reference genome. Quantification of gene expression was done using FeatureCounts tool to count reads mapped to genes. DEseq2 packages in R was used for normalization and count data's variance stabilization. Differential expression analysis has been done using DESeq2, which identify differentially expressed genes by using negative binomial distribution to model count data. FDR (False discovery rate, also called Benjamini-Hochberg procedure) was chosen as a multiple testing correction method to control the false discovery rate when conducting multiple comparisons. Gene Ontology enrichment analysis and KEGG pathway analysis has been done for functional enrichment analysis.

2.8.3 JC-1 Fluorescence Imaging

The mitochondrial membrane potential was assessed by calculating the ratio of red to green fluorescence intensity of JC-1 in individual cells. Statistical analysis was performed using GraphPad Prism 9 software. Differences between treated and control groups were analyzed using an repeated measures one-way ANOVA, with p-values < 0.05 considered statistically significant.

2.8.4 MitoTracker Green Fluorescence Imaging

Mitochondrial localization and morphology were analyzed by examining the distribution of MitoTracker Green fluorescence. Statistical analysis was performed using GraphPad Prism 9 software. Differences between treated and control groups were analyzed using an repeated measures one-way ANOVA, with p-values < 0.05 considered statistically significant.

Chapter 3

3 Results

3.1 Gene expression of mitochondria related genes after SR-18292 treatment

To determine the optimal concentration and duration of SR-18292 treatment, we performed real time PCR analyses of IMACs for known PGC1α target genes. Figure 3.1 illustrates the relative normalized expression levels of genes *Esrra Mpc2, Nrf1*, and *Tfam* after 6 hours of treatment with SR-18292, a PGC1α inhibitor, at concentrations of 5 µM, 10 µM, and 20 µM. The expression levels were normalized to *Actb*. Kruskal-Wallis test with multiple comparisons was used for statistical analysis and result showed no significant decrease in the expression of any of the genes across all concentrations. Therefore, 6 hours of exposure to SR-18292 was not enough to significantly influence the expression of these mitochondrial related genes.

As shown in Figure 3.2, cells treated with SR-18292 for 24 hours exhibited changes in gene expression levels. At 10 µM, there was significant downregulation of *Mpc2* and *Nrf1*, indicated by $*P<0.05$ and $**P<0.01$. However, *Esrra* and *Tfam* showed only slight changes in expression levels that were not statistically significant. This indicates that 24-hour exposure to SR-18292 at a moderate concentration specifically affects the expression of *Mpc2* and *Nrf1*.

Figure 3.3 displays the effects of prolonged exposure (72 hours) to SR-18292 on gene expression. At 5 µM, there was significant downregulation of *Esrra, Nrf1*, and *Tfam* (all $*P<0.05$), with *Mpc2* showing a slight, non-significant downregulation. Additionally, 10 µM SR-18292 led to significantly decreased expression of *Esrra* and *Nrf1* ($**P<0.01$). Therefore 72 hours of exposure to SR-18292, even at lower concentrations as 5 µM, significantly suppresses the expression of genes related to mitochondrial metabolism.

Overall, SR-18292 affects the expression of mitochondrial related genes in a time-dependent manner. While there were no significant changes at 6 hours after treatment, significant down-regulation was observed at 24 and 72 hours, particularly for *Mpc2* and

Nrf1 at 24 hours, and *Esrra, Nrf1*, and *Tfam* at 72 hours. Based on this result, we decided to use 5 µM SR-18292 for 72 hours for the following experiments.

t=6h

Figure 3.1 Expression level of genes involved in mitochondrial metabolism after 6 hours of SR-18292 use.

Bar graph showing relative normalized expression of *Esrra, Mpc2, Nrf1*, and *Tfam* transcript in the experimental group compared to control groups. Cells were harvested after 6 hours of SR-18292 use. SR-18292 was used in 3 concentrations, 5μM 10μM, and 20μM. No gene showed significant decrease in gene expression. Gene expression was normalized to *Actb* and Kruskal Wallis test with multiple comparisons was used for statistical analysis. N=6; *P<0.05, **P<0.01.

t=24h

Figure 3.2 Expression level of genes involved in mitochondrial metabolism after 24 hours of SR-18292 use.

Bar graph showing relative normalized expression of *Esrra, Mpc2, Nrf1*, and *Tfam* transcript in the experimental group compared to control groups. Cells were harvested after 24 hours of SR-18292 use. SR-18292 was used in 3 concentrations, 5μM, 10μM, and 20μM. *Mpc2* and *Nrf1* were significantly downregulated with SR-18292 10uM use while *Esrra* and *Tfam* showed slight change. Gene expression was normalized to *Actb* and Kruskal Wallis test with multiple comparisons was used for statistical analysis. N=6; *P<0.05, **P<0.01.

t=72h

ESRRa

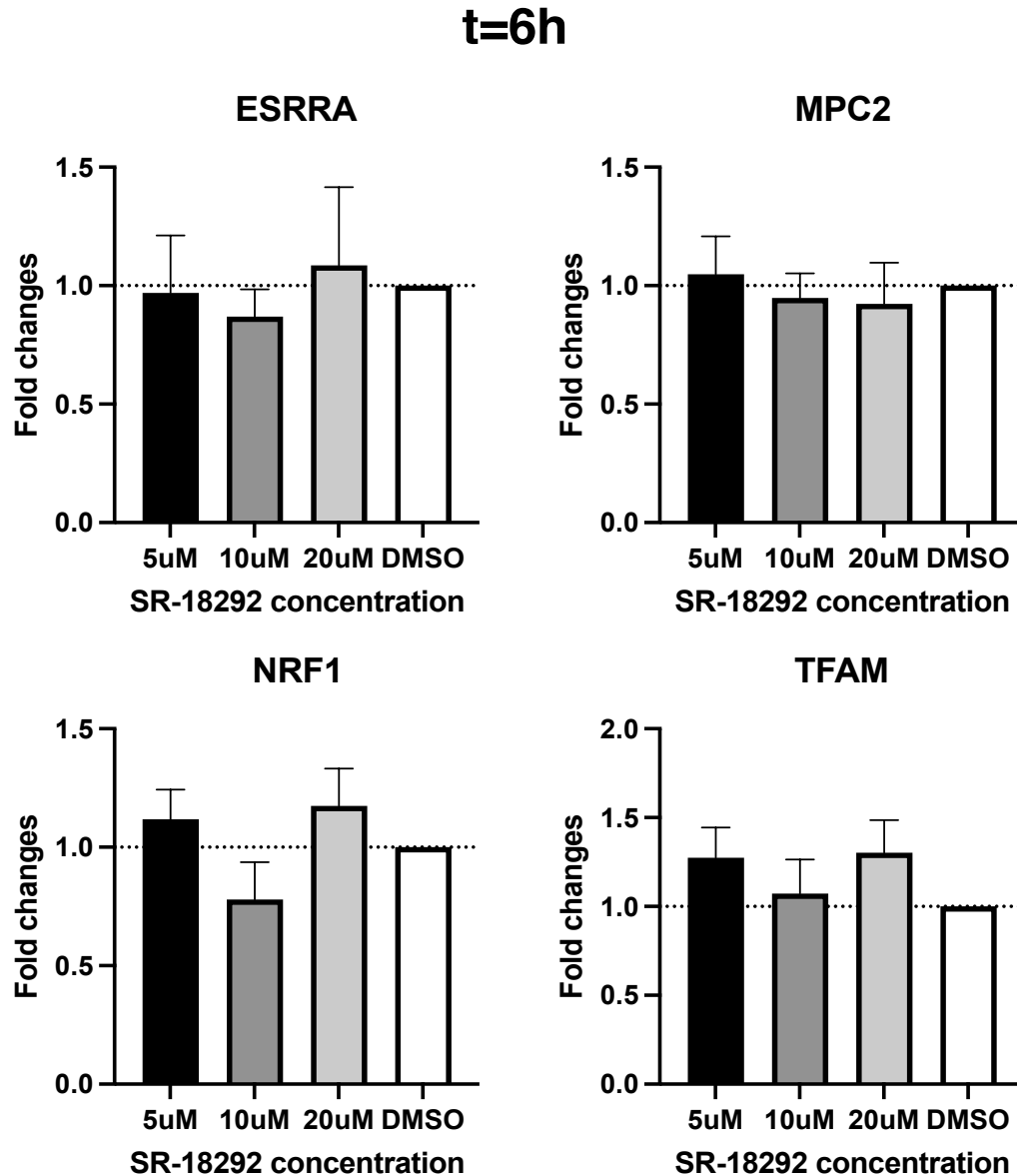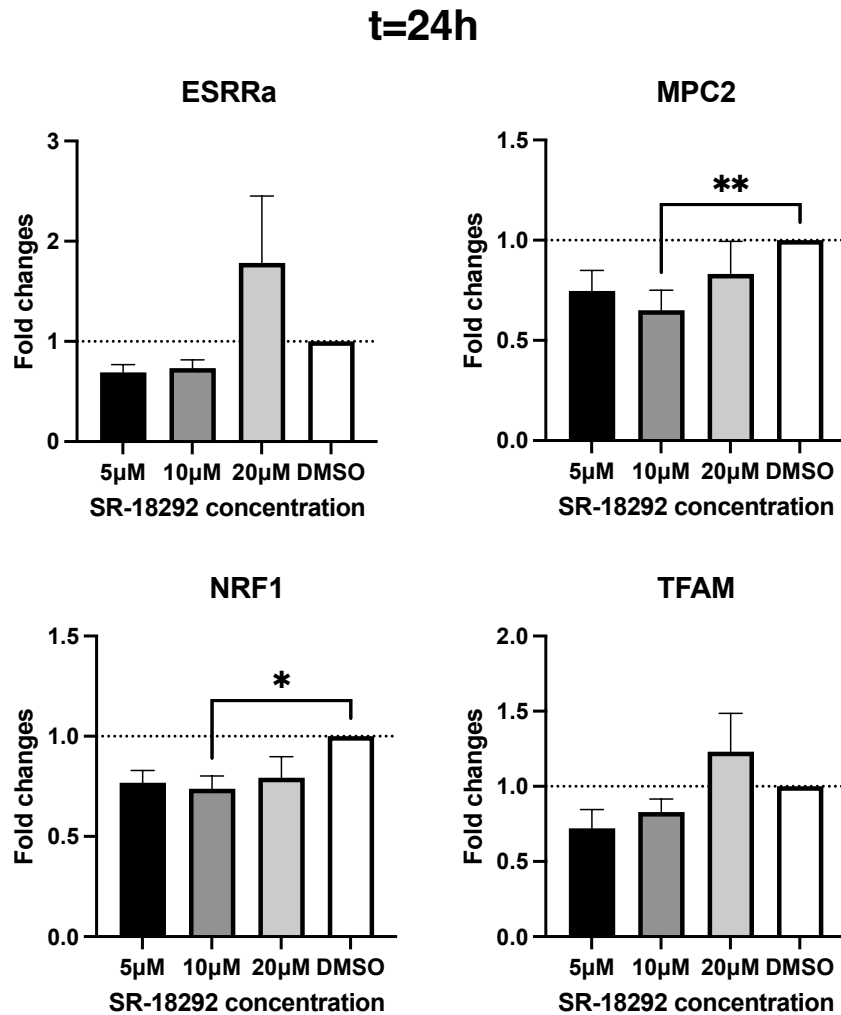
MPC2

NRF1

TFAM

Figure 3.3 Expression level of genes involved in mitochondrial metabolism after 72 hours of SR-18292 use.

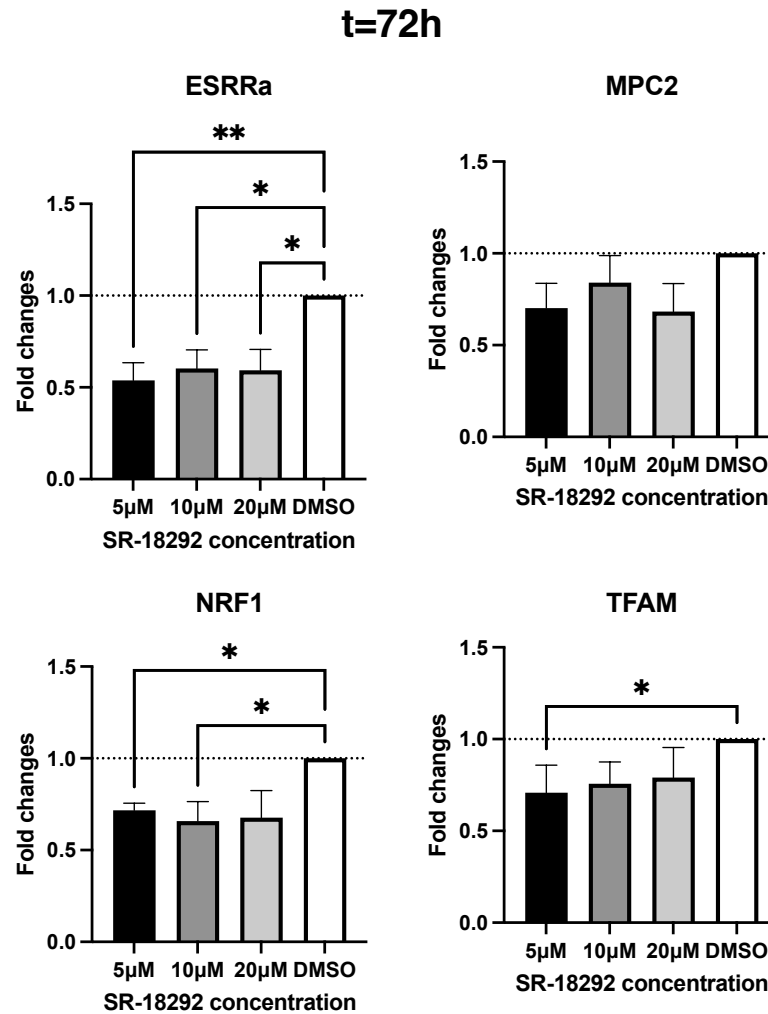Bar graph showing relative normalized expression of Esrra, Mpc2, Nrf1, and Tfam transcript in the experimental group compared to control groups. Cells were harvested after 72 hours of SR-18292 use. SR-18292 was used in 3 concentrations, 5µM, 10µM, and 20µM. SR-18292 5uM showed significant downregulation in Esrra, Nrf1 and Tfam while slight downregulation in Mpc2. Also, Esrra and Nrf1 showed significantly decreased expression with 10uM use of drug. Gene expression was normalized to Actb and Kruskal Wallis test with multiple comparisons was used for statistical analysis. N=6; *P<0.05, **P<0.01.

3.2 RNA-seq Analysis of SR-18292 treated chondrocytes

RNA sequencing analysis was performed to compare the transcriptomic profiles between control and SR-18292 treated IMAC cells after 72 hours of exposure to a 5 µM concentration of the PGC1α inhibitor. The results highlight significant changes in gene expression and pathway involvement, which are detailed across four main figures.

Four trials were sequenced by London Regional Genomics Centre, but only three trials were used for further analysis based on PCA result. (Supplement figure 3) PCA result showed that there was more similarity within each trial rather than control compared to treatment group. Trial 5 showed different pattern compared to other trials 1,3 and 4 thus, we decided to include only trial 1,3, and 4 for further expression analysis.

The volcano plot primarily helps in identifying and visualizing significantly differentially expressed genes. Volcano plot in Figure 3.4, showing upregulated and downregulated DEGs between the control and treated cells. Among 1494 genes with at least a 1.5-fold change, 82 DEGs are established as statistically significant with a p-value under 0.05. All significantly changed gene list is showed in supplement figure 2. This visualization emphasizes the strong impact of SR-18292 on gene expression in IMAC cells where cellular processes are hugely changed by this treatment.

Figure 3.5 shows KEGG (Kyoto Encyclopedia Genes and Genomes) pathways enriched among the differentially expressed genes. The KEGG enrichment analysis is a hard-core method for functional extrapolation of differentially expressed genes and their involvement in biological systems and processes. It shows pathways on the y-axis, while on the x-axis there are the enrichment factor and the bubble size, which indicates the number of genes involved, with the color intensity changing with the corrected p-value. These showed that fourteen pathways were enriched significantly (p-value less than 0.05), claiming the fact that SR-18292 contributes to metabolic and signaling pathways vital for normal cell functioning and homeostasis.

The GO analysis classifies genes and products into three major functional domains, namely: Biological Process (BP), Molecular Function (MF), and Cellular Component

(CC). GO analysis aids in understanding the role of genes and interaction within the context of biological systems. Enriched ontology term analysis for the genes showing a 1.5-fold change revealed the key biological processes affected by the SR-18292 treatment (Figure 3.6). Enriched terms were then statistically hierarchically tree-arranged according to kappa-statistical similarities of their gene memberships: A kappa score threshold of 0.3 was used for defining distinct clusters out of 100. From the top 20 resultant clusters, very strong representation related to muscle system processes gives, again, an indication that the SR-18292 may regulate cellular functions related to muscle or movement.

Gene Set Enrichment Analysis (GSEA) is an analytical approach that describes the features characteristic of particular sets of genes. It is widely applied in downstream analysis of RNA-seq data. GSEA is very useful, as it is able to find subtle but coordinated changes in gene expression that are not evident from the analysis of individual genes. It is frequently used in genomic studies to understand the biological processes, pathways, and molecular mechanisms that underlie given conditions or interventions. GSEA (Figure 3.7) analysis was conducted to uncover the biological significance of the identified differential expression. In the ES plots, one finds that specific gene sets are enriched in the highest upregulated or downregulated genes in cells treated with SR-18292. Mainly, the data are responsible for the major enrichment signals of the leading-edge genes in these sets, suggesting an oriented impact of SR-18292 on a restricted number of biological pathways and functions.

Additional qPCR was performed with genes from DEG down-regulated and up-regulated gene list. Primers for selected genes, *Pouf2f2, Slc22a3, Pmaip1, Cxcl13, Slc22a3* and *Sp110*, were designed (Table 2.2). *Pla2g4b* was excluded from further experiment by showing visible off-target binding or primer dimers. *Pouf2f2, Slc22a3, Sp110, Cxcl13*, and *Pmaip1* primer pairs didn't have visible off-target binding or primer dimers and had an optimal annealing temperature of 60°C. The efficiency and specificity of these primers were tested with a standard curve. Among 5 genes, only *Slc22a3* and *Sp110* showed acceptable efficiency (Supplement figure 1). Therefore, designed primers for *Slc22a3, Sp110* and additional four selected genes (*RORa, PDK4, Col10a1, SOX9*) known as involved in the development, maintenance, repair, and metabolic processes of cartilage

were used for qPCR. RNA was extracted from primary chondrocyte treated with 5μM, 10μM, 20μM concentration of SR-18292 for 6 hour, 24 hour and 72 hour. *Actb* was used as reference gene to normalize the gene expression level. qPCR result (Supplement figure 2) showed that all genes except *Col10a1* are showing highly up regulated with 20μM 72hr inhibitor use.
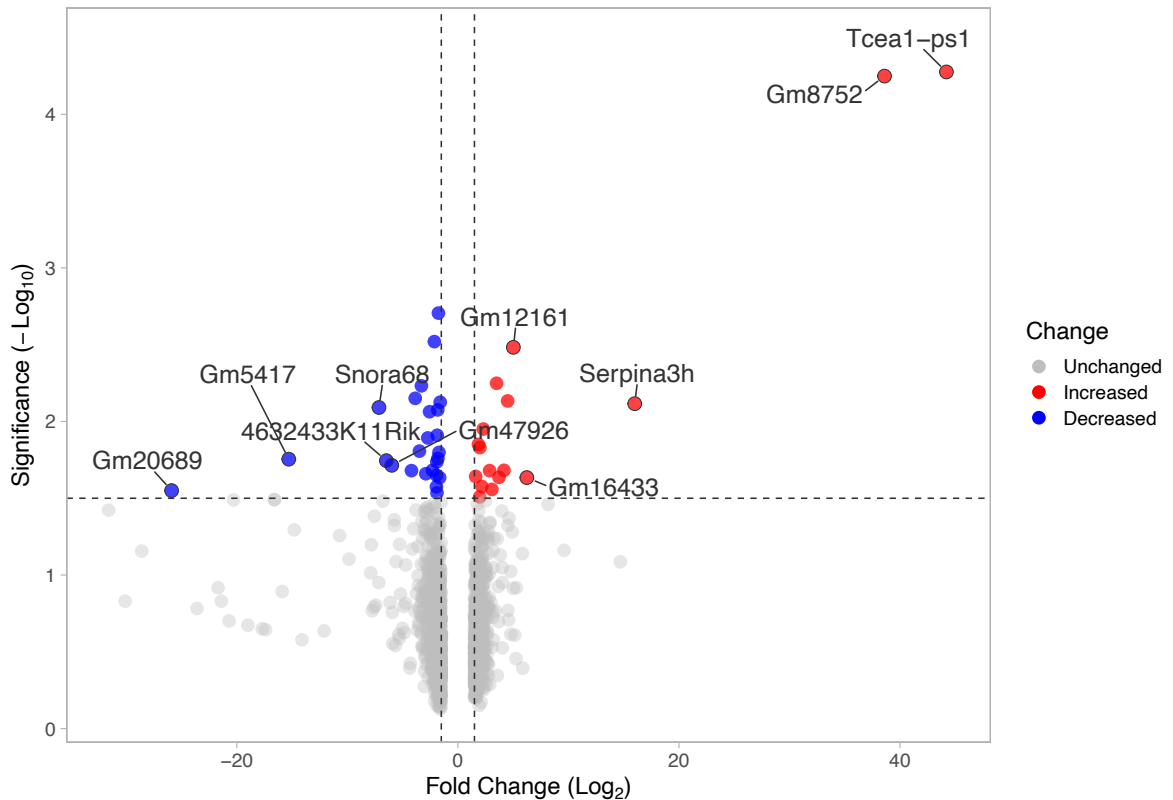
Figure 3.4 Volcano plot with 1.5-fold change gene list

Volcano plot for both upregulated and downregulated differentially expressed genes (DEGs) from comparison of control IMAC cells with PGC1α inhibitor treated IMAC cells. Cells were harvested after 72 hours of 5uM SR-18292 use. Among 1494 genes showing at least 1.5-fold change in gene expression, 82 genes were selected based on p value under 0.05.
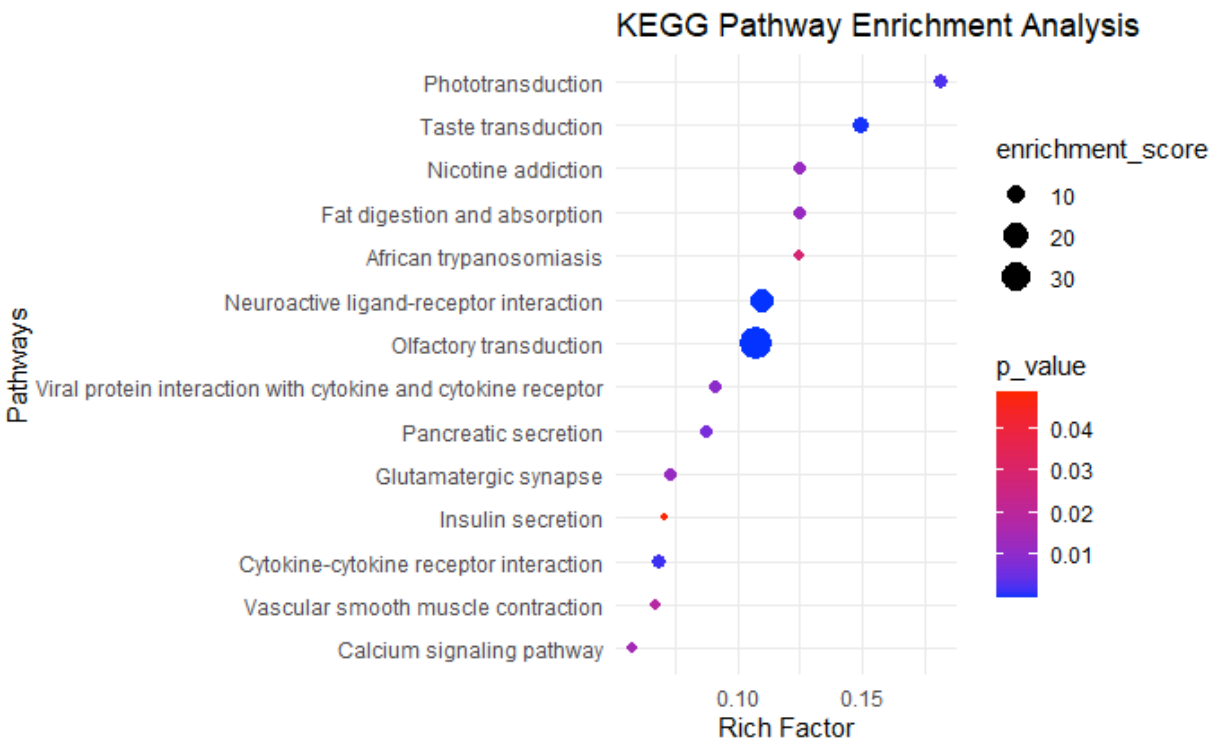
Figure 3.5 KEGG Pathway Enrichment Analysis

Pathway enrichment of differentially expressed genes. y-Axis indicates the pathway name and x-axis indicates the enriched factor in each of pathways. The bubble size indicates the number of genes. The color bar indicates the corrected p-value, the red represents higher value, the blue represents lower value. 14 pathways were selected among 243 pathways based on p value under 0.05.
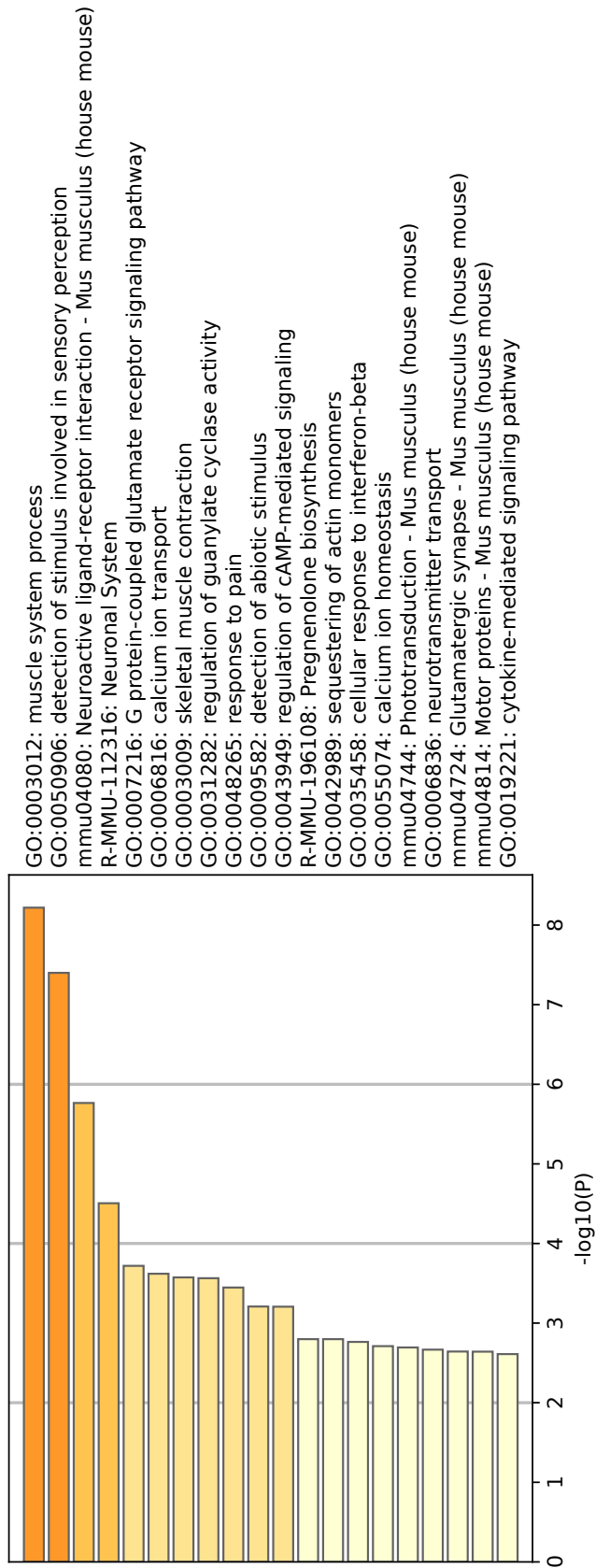
Figure 3.6 Enriched ontology clusters across 1.5 fold change gene list

All statistically enriched terms accumulative hypergeometric p-values and enrichment factors were calculated and used for filtering. Remaining significant terms were then hierarchically clustered into a tree based on Kappa-statistical similarities among their gene memberships. Then 0.3 kappa score was applied as the threshold to cast the tree into term clusters. Top 20 clusters including Muscle system process are showed among 375 GO terms which showed p value < 0.05.
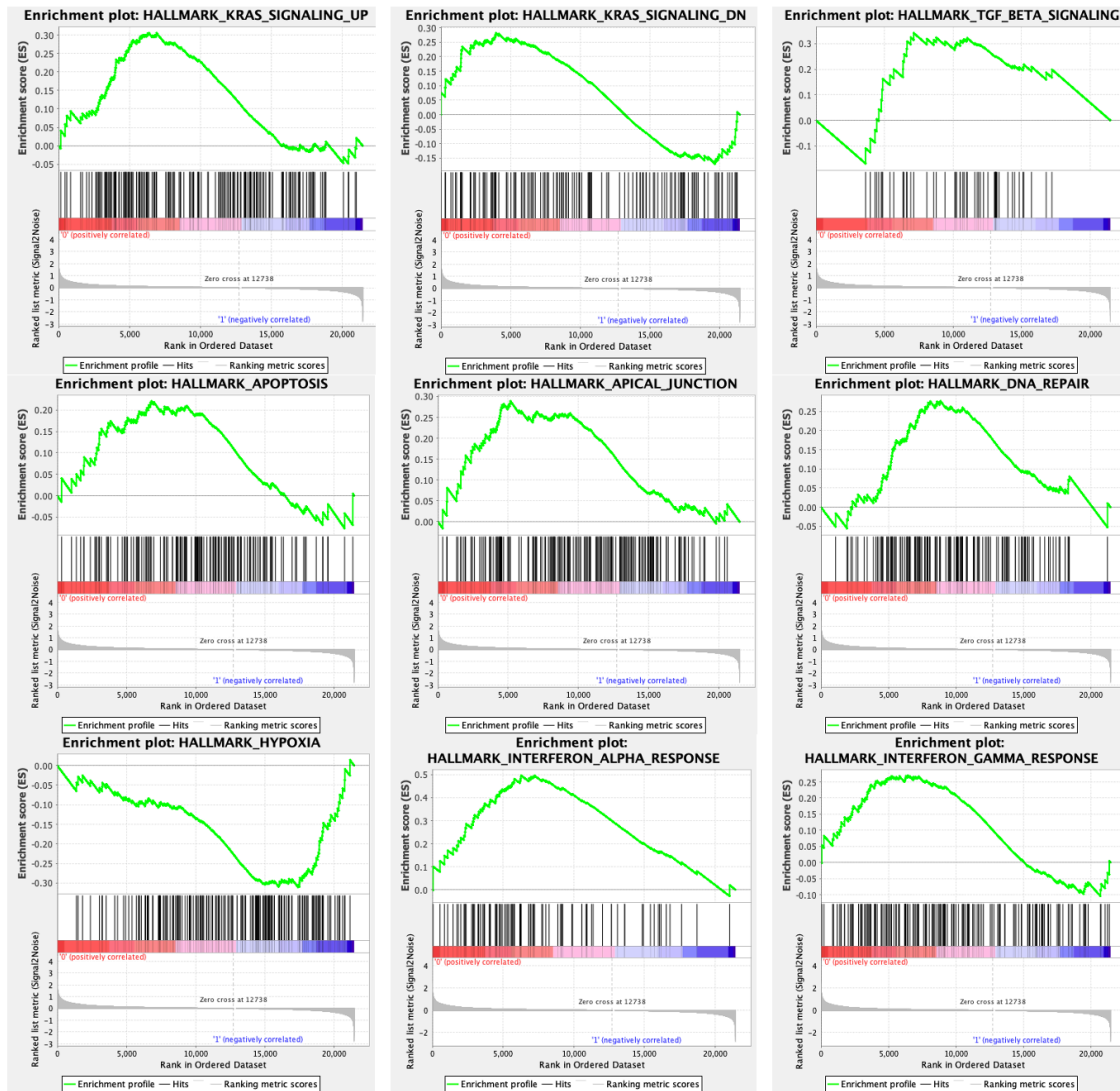
Figure 3.7 Gene Set Enrichment analysis

Enrichment score (ES) plots for the indicated gene sets. Negative and positive ES values point to gene sets over-represented in the top most down-or up-regulated genes in SR-18292 treated IMAC cells. Vertical bars refer to individual genes in a gene set and their position reflects the contribution of each gene to the ES. Genes that belong to the leading-edge subset contribute to the enrichment signal.

3.3 Impact of SR-18292 on Mitochondria in Primary Chondrocytes

3.3.1 Qualitative Analysis of Mitochondrial Membrane Potential using JC-1

The level of the mitochondrial membrane potential of IMACs treated with SR-18292 in 4 different timepoints were plotted in Figure3.1(a). JC-1 fluorescence dye, which aggregates mitochondrial membrane potential ($\Delta\Psi$m), was used to measure mitochondrial membrane potential. In healthy, unstressed mitochondria, JC-1 accumulates in high concentrations and emits red fluorescence, while in damaged or depolarized mitochondria, it accumulates at lower concentrations and emits green fluorescence. Thus, JC-1 staining is particularly useful for assessing the functional state of mitochondria.

In 0 hour and 6 hour, there are no significant changes in the red to green fluorescence ratio, which indicates that short-term exposure to SR-18292 does not markedly affect mitochondrial membrane potential (Figure 3.8 (a)). Meanwhile at 24 hour and 72 hours, a significant decrease of red to green fluorescence ratio was observed in SR-18292 treated chondrocytes compared to control. This suggests that inhibition of PGC1α decrease mitochondrial membrane potential. Statistical analysis using Repeated Measures One-Way ANOVA were used to confirm significance. (*P<0.05).

Fluorescence images of control (Figure 3.8 (b)) and SR-18292 treated chondrocytes (Figure3.1(c) stained with JC-1 showed different fluorescence. Figure 3.1(b) shows intensive red fluorescence from control chondrocytes, which indicates that it has high mitochondrial membrane potential. Figure 3.1(c) shows chondrocytes treated with 5 µM SR-18292 for 72 hours and showing predominantly green fluorescence. It indicates a significant decrease in mitochondrial membrane potential.

Therefore, we confirmed that treatment with SR-18292 induced a time-dependent decrease in mitochondrial membrane potential in primary chondrocytes. While no significant effects were observed at 0 and 6 hours, 24 hour and 72 hour showed a significant reduction in the mitochondrial membrane potential. This suggests that PGC1α

plays a crucial role in maintaining mitochondrial function in chondrocytes, and its inhibition by SR-18292 disrupts this function over time.
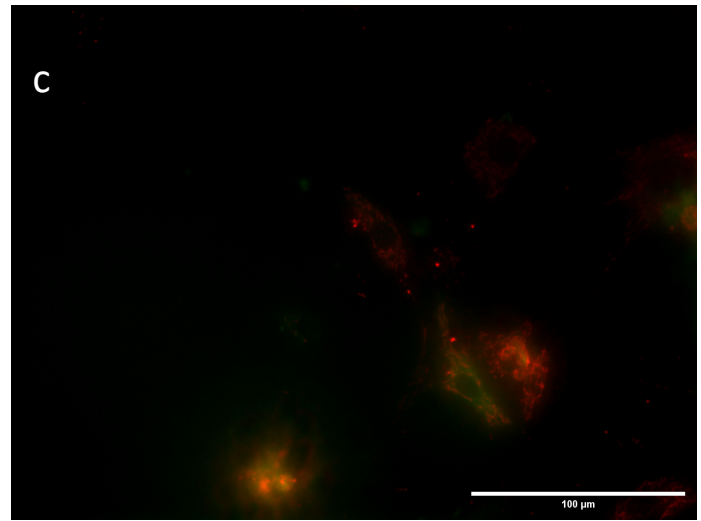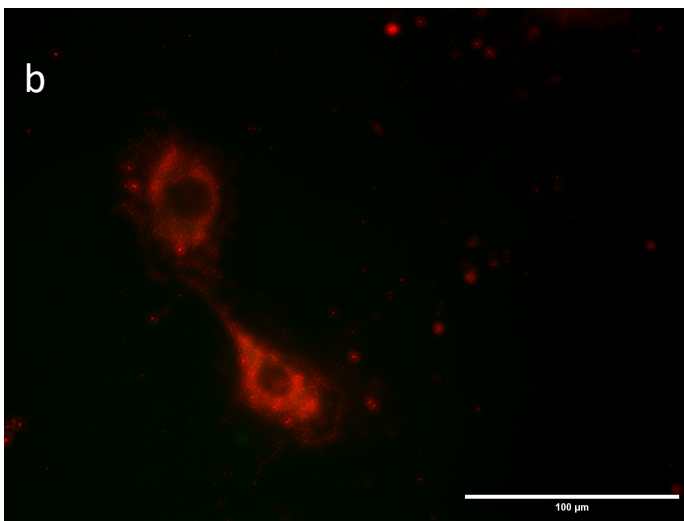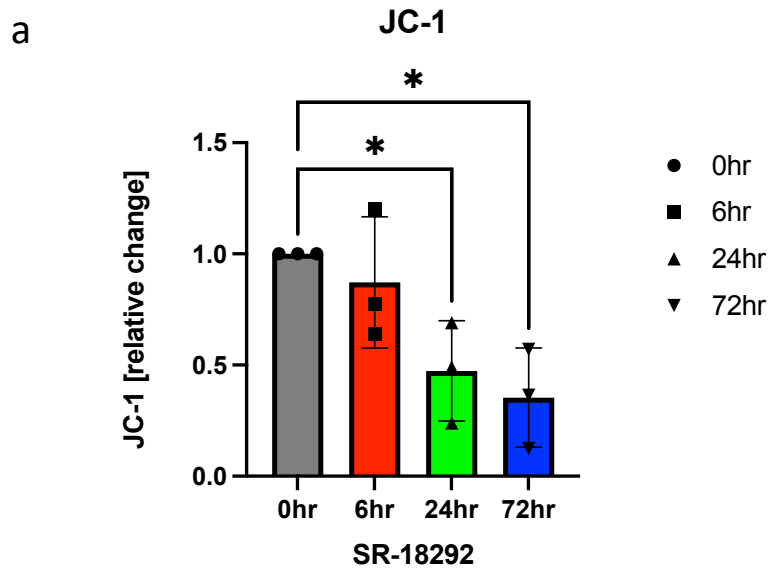
Figure 3.8 Quantification of mitochondrial membrane potential of primary chondrocytes

(a) The red to green ratio was significantly reduced in the presence of the PGC1α inhibitor SR-18292 compared to control chondrocytes after 24 hours and 72 hours. Repeated Measurement one-way ANOVA was performed. (b)(c) Fluorescence image of control and SR-18292 treated chondrocytes isolated at P15 stained with JC-1. (b)Intense red stain of control chondrocytes clearly indicated a higher mitochondrial membrane potential compared to (c) green fluorescence SR-18292 72 hour treated chondrocytes. Scale bar = 100 µm; JC1 staining N = 3 for each timepoint; *P<0.05.

3.4.2 Mitochondrial Mass Quantification in Primary Chondrocytes Treated with SR-18292

The assessment of the mass of mitochondria was done using quantitative analysis on chondrocytes treated with 5 µM concentration of SR-18292 at 6, 24, and 72 hours.

Figure 3. 9(a) displays the MitoTracker Green staining which demonstrates that there were no changes in the intensity of the chondrocytes' fluorescence between the control group and the chondrocytes samples exposed to SR-18292 for 6 and 24 hours. However, significant decrease in the mitochondrial mass was found at the 72 hours in the SR-18292 treated group compared to the control group. Repeated measurement one way ANOVA was used for statistical analysis to confirm significance. This suggests that SR-18292 might disturb mitochondrial biogenesis or induce mitochondrial degradation by inhibiting PGC1α over an extended treatment period.

Figure 3.2(b) shows fluorescence image of control chondrocytes and Figure 3.2(c) shows chondrocytes treated with 5 µM SR-18292 for 72 hours.

Therefore, we concluded that SR-18292 decrease mitochondrial membrane potential as well as mitochondrial mass. Inhibition of PGC1α results in negative influence to functional health, shape and distribution of mitochondria in chondrocytes.

a

Mitotracker Green

MitoTracker [relative change]

- ● 0hr
- ■ 6hr
- ▲ 24hr
- ▼ 72hr

SR-18292

b

c

100 µm

100 µm
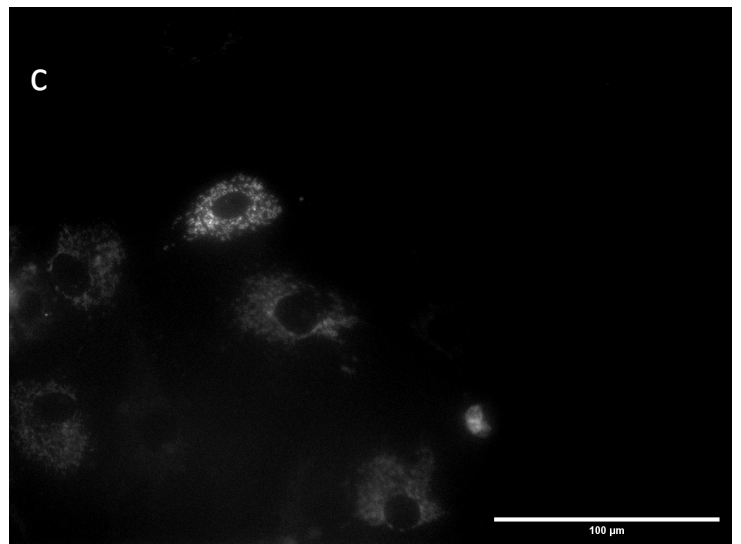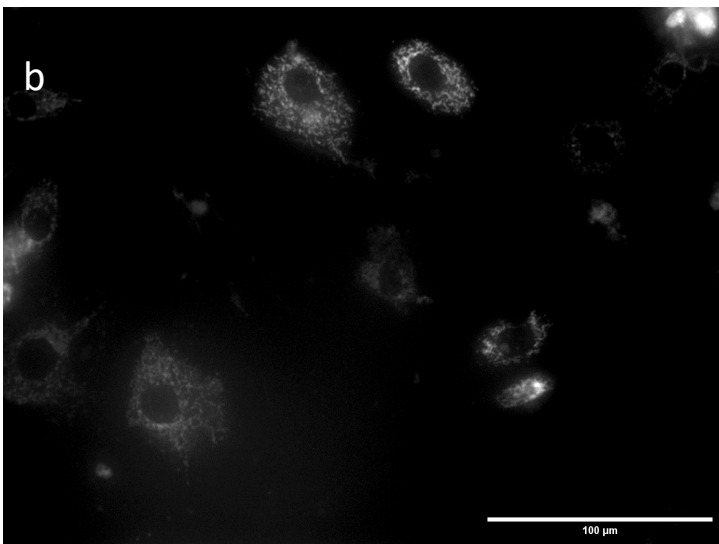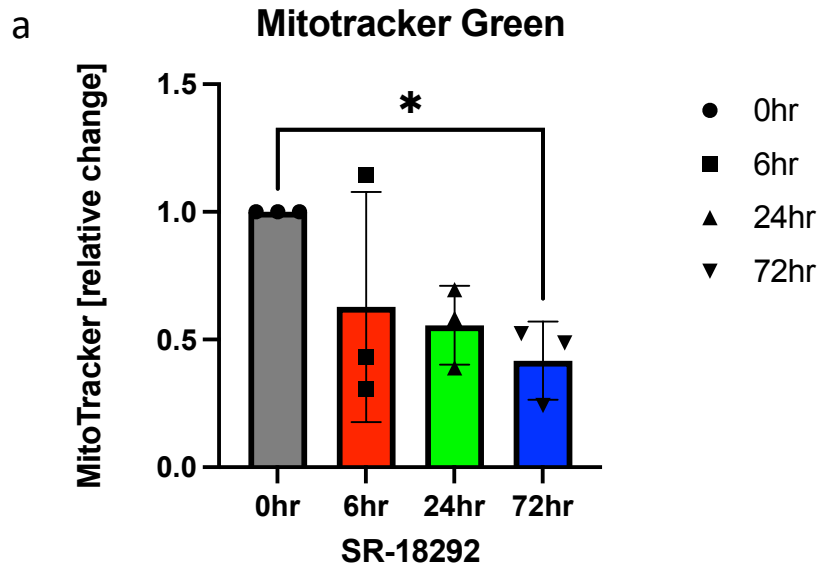
Figure 3.9 Quantification of mitochondrial mass of primary chondrocytes

    (a) Mito Tracker Green staining of isolated chondrocyte revealed time-dependent differences between control and SR-18292 treated chondrocytes. SR-18292 was added to IMAC cells for 6, 24, and 72 hours with 5uM concentration. 72 hours group showed statistically significant compared to control group. Repeated Measurement one-way ANOVA was performed. (b)(c) Fluorescence image of control and SR-18292 treated chondrocytes isolated at P15 stained with MitoTracker Green. (b) 0hr control. (c) 72hr use of SR-18292. Scale bar = 100 µm; MitoTracker Green N = 3 for each timepoint.

<div align="center">

Chapter 4

</div>

4   Discussion

In this study, we investigated the effects of SR-18292, a PGC1α inhibitor, on mitochondrial function and gene expression in primary chondrocytes. Our qPCR analysis revealed that while no significant changes were observed at 6 hours post-treatment (Figure 3.1), prolonged exposure (24 and 72 hours) led to significant down-regulation of mitochondrial-related genes such as *Esrra, Nrf1,* and *Tram*, particularly at a 5 µM concentration (Figure 3.2 and Figure 3.3). Interestingly, the 5 µM concentration at 72 hours proved to be more effective than higher concentrations, suggesting a concentration-dependent effect of SR-18292 on mitochondrial function.

The observed down-regulation of genes related to mitochondrial metabolism can be attributed to the inhibitory effects of SR-18292 on PGC1α. Previous studies have shown that PGC1α is crucial for maintaining mitochondrial biogenesis and metabolism. Inhibition of PGC1α by SR-18292 disrupts these processes, leading to impaired mitochondrial function and increased cell death. In neuronal PC12 cells, high concentration of SR-18292 induced a reduction of the percentage of cells with neurites by 10% (Wenting, 2024). Our qPCR results, which is indicating the highest inhibitory effect at 5 µM for 72 hours of SR-18292 use, align with findings that high concentrations of SR-18292 possibly induce cell death or damage. This suggests that lower concentrations over extended periods may be more effective in inhibiting PGC1α without inducing excessive cytotoxicity.

Our RNA-seq analysis revealed significant changes in gene expression upon SR-18292 treatment, particularly in pathways related to cellular stress response, regulation of cell fate or interconnected signaling networks. Since PGC1α is highly expressed in oxidative tissues such as heart, muscle, kidney, and brain, this gene is involved in various cellular signaling pathways.

Figure 3.5 illustrates the KEGG pathway enrichment analysis, identifying fourteen significantly enriched pathways among the differentially expressed genes. The enrichment of specific KEGG pathways in the inhibition of PGC1α indicates a potential regulatory role of PGC1α in these pathways, especially those related to sensory signaling, immune response, and cellular interactions.

Pathways related to sensory signaling such as olfactory transduction, taste transduction, phototransduction might indicate that inhibition of PGC1α altered sensory perceptions or signaling changes in response to environmental cues, although the roles of these pathways in primary chondrocytes are unclear.

Also, pathways related to neurotransmission also enriched, such as neuroactive ligand-receptor interaction and the glutamatergic synapse. This is consistent with previous studies showing that PGC1α plays important roles in neuronal functions (Virga, 2024). Also, PGC1α has been identified as an activity-dependent signaling pathway in neurons (Virga, 2024) and shown to maintain cerebral neuron function by regulating mitochondrial function (Jain, 2021). Furthermore, enrichment of cytokine-cytokine receptor interaction, viral protein interaction with cytokine-cytokine receptor pathways is indicating that PGC1α is crucial in immune related response, which align with previous research (Gerbec, 2021).

In addition, calcium signaling was also enriched under inhibition of PGC1α. Calcium signaling pathway is essential for numerous cellular processes, including muscle contraction, neurotransmission, and cell division. Research (Wu, 2002) revealed that the regulation of mitochondrial biogenesis in skeletal muscle by CaMK, highlighting a calcium-regulated signaling pathway that controls mitochondrial biogenesis in mammalian cells. The changes observed in these pathways may reflect disruptions in cellular communication and signaling cascades, which are essential for maintaining cellular homeostasis and proper physiological responses.

Our enriched ontology clustering result (Figure 3.6) was corresponding with KEGG enriched analysis result. Pathways related to neuronal functions, sensory system, muscle related process, and immune response pathways were enriched and clustered in the top 20 clusters. Especially, muscle system process, skeletal muscle contraction, regulation of

muscle contraction, skeletal muscle adaptation, and regulation of skeletal muscle tissue regeneration were also included among 375 GO terms that showed p value under 0.05. The enrichment of these GO terms in the inhibition of PGC1α underscores its vital role in muscle physiology, from contraction and adaptation to regeneration. Disruptions in these processes due to the inhibition of PGC1α possibly highlight the importance of this regulator in maintaining muscle health and performance, offering potential targets for therapeutic intervention in muscle-related diseases and conditions. However, new study that address role of PGC1α in muscle cells is required to reveal potential targets in muscle-related diseases, since this study has been performed in chondrocytes.

PGC1α also involved in various cancer related pathways. PGC1α plays multifaceted roles in cancer metabolism, acting either as a tumor suppressor or an oncogenic factor depending on the cancer type. In some cancers, such as thyroid and renal cancer, PGC1α downregulation correlates with disease progression. Restoring its levels can inhibit cell proliferation and invasion, enhancing chemotherapy sensitivity. In other cancers like colorectal, gastric, and ovarian cancers, PGC1α overexpression supports tumor growth by promoting oxidative phosphorylation and mitochondrial function, aiding the cancer cells' adaptation to metabolic stress (Wang, 2024). GSEA analysis (Figure 3.7) correspond to these findings. GSEA result showed that differentially expressed genes in SR-18292 treated group are involved in pathways such as apoptosis, hypoxia, DNA repair, TGF-beta etc. Most of the pathways identified in the GSEA analysis were related to cancer pathways, cellular stress response, regulation of cell fate, or interconnected signaling networks. It aligns with the findings above.

We also confirm how inhibition of PGC1α by treating with 5μM SR-18292 affect mitochondrial morphology. JC-1 and MitoTracker Green fluorescence dye were used to identify any changes in mitochondrial membrane potential and mitochondrial mass respectively. In healthy mitochondria, JC-1 accumulates in high concentrations and emits red fluorescence (J-aggregates). In damaged or depolarized mitochondria, JC-1 accumulates at lower concentrations and emits green fluorescence (J-monomers). Thus, JC-1 is particularly useful for assessing the functional state of mitochondria.

Figure 3.8 (a) showed that under inhibition of PGC1α, there was significant change of mitochondrial membrane potential, especially in 24 hour and 72 hour use of SR-18292. Also in fluorescent image, intense red signal was shown in control chondrocyte (Figure 3.8 (b)), while 5μM 72 hour inhibitor treated chondrocyte showed strong green signal. It indicates that inhibition of PGC1α activity can cause mitochondrial damage in membrane potential manner.

MitoTracker Green is used to stain mitochondria and is useful for observing the amount and distribution of mitochondria in cells. Unlike some other mitochondrial dyes, MitoTracker Green binds to mitochondria regardless of the mitochondrial membrane potential, meaning it can stain mitochondria whether they are functional or not. It is used to reveal presence and quantity of mitochondria within the cell. In our MitoTracker Green result (Figure 3.9) also showed there was significant decrease of mitochondrial mass under use of 5μM SR-18292. Figure 3.9 (a) showed significance in inhibitor treated group for 72 hour. It indicates that SR-18292 can also affect mitochondrial mass, shape and distribution. Overall, our fluorescence imaging of primary chondrocyte suggests that use of SR-18292 can occur inhibition of PGC1α activity which results in decreasing mitochondrial functional health and distribution. This possibly can influence survival and function of chondrocyte, since mitochondria are essential organelle in cells.

Limitations and figure directions

A limitation of this study is the specificity of SR-18292 for PGC1α. Although it is known to inhibit PGC1α, and frequently used as PGC1α inhibitor, its effects on other coactivators like PGC1β or PRC have not been thoroughly investigated. Its lysine acetylation domain, which is target domain of SR-18292 for inhibition, is a shared domain in PGC1α and other coactivators, off target effect can occur. In this case inhibitor may bind to and inhibit other proteins or enzymes that have similar structures or active sites such as PGC1β or PRC. This can lead to the disruption of other crucial biological pathways that are not intended to be targeted, causing broad and unpredictable biological effects. Non-specific PGC1α inhibitors can lead to unintended pathway modulation, toxicity, reduced efficacy, complex biological responses, increased resistance, and immune modulation, ultimately

compromising the safety and effectiveness of the treatment. Therefore, future studies should include binding assays and gene expression analyses to confirm the specificity of SR-18292. Ideally, key experiments will be repeated in cells where PGC1α is inhibited genetically.

Another limitation of this study is the sample size (n=3) for RNA-seq and mitochondrial morphology experiments was small, which might affect the robustness of the results. Using a small sample size such as n=3 in an experiment can lead to a range of problems including lack of statistical power, high variability, reduced generalizability, and misleading effect sizes (Button, 2013).

 Additionally, the use of bulk RNA-seq instead of single-cell RNA-seq can sometimes show more differences between trials rather than between control and treatment groups due to biological variability and batch effect. Biological variability can be affected by outliers and noise. Outliers in the data, whether due to biological variability or technical errors, can disproportionately affect the results. If not properly identified and managed, outliers can skew the analysis. In our PCA result (Supplement figure 3), trial 5 showed as outlier and was removed from analysis. This might also cause biological variability. Increasing sample size can be helpful to resolve this problem. High levels of noise in the RNA-seq data can also obscure true biological differences. Noise can be introduced at various stages, from sample collection to sequencing (Liu, 2014). Differences in sample processing batches can introduce systematic biases. Batch effects occur when samples are processed at different times, by different technicians, or with different reagents, leading to variations that are unrelated to the biological conditions being studied (Leek, 2010).

Lastly, DMSO only treated group for each timepoints (6hr, 24hr and 72hr) could be added as vehicle in fluorescence imaging to clarify that changes between control and inhibitor treated group was only affected by inhibitor, but not other factors such as cellular stress from adhering on 96 well plate for longer time.

 In conclusion, our research showed that SR-18292 effectively inhibits PGC1α, impacting mitochondrial function and gene expression in primary chondrocytes. Further research is needed to confirm its specificity and to explore its potential therapeutic applications in OA involving mitochondrial dysfunction.

References

Cowan, D., 2010. Oral Aloe vera as a treatment for osteoarthritis: a summary. British Journal of Community Nursing, 15(6), pp.280-282.

Sarzi-Puttini, P., Cimmino, M.A., Scarpa, R., Caporali, R., Parazzini, F., Zaninelli, A., Atzeni, F. and Canesi, B., 2005, August. Osteoarthritis: an overview of the disease and its treatment strategies. In Seminars in arthritis and rheumatism (Vol. 35, No. 1, pp. 1-10). WB Saunders.

Wu, L., Liu, H., Li, L., Liu, H., Cheng, Q., Li, H. and Huang, H., 2014. Mitochondrial pathology in osteoarthritic chondrocytes. Current drug targets, 15(7), pp.710-719.

Srivastava, S., 2017. The mitochondrial basis of aging and age-related disorders. Genes, 8(12), p.398.

Zheng, L., Zhang, Z., Sheng, P. and Mobasheri, A., 2021. The role of metabolism in chondrocyte dysfunction and the progression of osteoarthritis. Ageing research reviews, 66, p.101249.

Flachs, P., Horakova, O., Brauner, P., Rossmeisl, M., Pecina, P., Franssen-van Hal, N., Ruzickova, J., Sponarova, J., Drahota, Z., Vlcek, C. and Keijer, J., 2005. Polyunsaturated fatty acids of marine origin upregulate mitochondrial biogenesis and induce β-oxidation in white fat. Diabetologia, 48, pp.2365-2375.

Zhang, Q., Lei, Y.H., Zhou, J.P., Hou, Y.Y., Wan, Z., Wang, H.L. and Meng, H., 2019. Role of PGC-1α in mitochondrial quality control in neurodegenerative diseases. Neurochemical research, 44, pp.2031-2043.

Nishimura, R., Hata, K., Takahata, Y., Murakami, T., Nakamura, E. and Yagi, H., 2017. Regulation of cartilage development and diseases by transcription factors. Journal of bone metabolism, 24(3), pp.147-153.

Zhao, X., Petursson, F., Viollet, B., Lotz, M., Terkeltaub, R. and Liu-Bryan, R., 2014. Peroxisome proliferator–activated receptor γ coactivator 1α and FoxO3A mediate chondroprotection by AMP-activated protein kinase. Arthritis & rheumatology, 66(11), pp.3073-3082.

Arden, N. K. and NEVITT, M. (2006). Osteoarthritis: epidemiology. Best Practice &Amp; Research Clinical Rheumatology, 20(1), 3-25.

Park, D. R., Choi, B. R., Yeo, C., Yoon, J. E., Hong, E. Y., Baek, S. H., … & Ha, I. (2024). Mume fructus reduces interleukin-1 beta-induced cartilage degradation via mapk downregulation in rat articular chondrocytes. Plos One, 19(5), e0302906.

Marks, R. (2017). Muscle and osteoarthritis joint status: current research highlights and their implications. SM Journal of Orthopedics, 3(1), 1-7.

Marks, R. (2020). Osteoarthritis and falls: is there a link?. Journal of Aging Research and Healthcare, 3(2), 1-13.

Stone, R. C. and Baker, J. (2015). Painful choices: a qualitative exploration of facilitators and barriers to active lifestyles among adults with osteoarthritis. Journal of Applied Gerontology, 36(9), 1091-1116.

Su, W., Liu, G., Mohajer, B., Wang, J., Shen, A., Zhang, W., … & Wan, M. (2022). Senescent preosteoclast secretome promotes metabolic syndrome associated osteoarthritis through cyclooxygenase 2. eLife, 11.

Shah, K., Cai, H., Lane, J. C. E., Collins, G. S., Arden, N. K., Furniss, D., … & Filbay, S. R. (2020). Prognostic factors for finger interphalangeal joint osteoarthritis: a systematic review. Rheumatology, 60(3), 1080-1090.

Mobasheri, A. and Levesque, M. C. (2019). Osteoarthritis (oa): a modern disease of the anthropocene era

Li, L., Liu, Z., Li, Y., Hu, X., Zhang, Y., & Fan, P. (2020). Profiling of inflammatory mediators in the synovial fluid related to pain in knee osteoarthritis. BMC Musculoskeletal Disorders, 21(1).

Sadri, Bahareh, Nouraein Sh, Nikoo Hossein-Khannazer, Javad Mohammadi, and Massoud Vosough. "Current and novel theranostic modalities for knee osteoarthritis." Сеченовский вестник 12, no. 3 (2021): 17-30.

Othman, S. F., Williams, J. M., Sumner, D. R., & Magin, R. L. (2004). Mri heterogeneity of articular cartilage in strong magnetic fields: dependence on proteoglycan content. Concepts in Magnetic Resonance Part B: Magnetic Resonance Engineering, 23B(1), 33-43.

Zheng, S., Xia, Y., & Badar, F. (2010). Further studies on the anisotropic distribution of collagen in articular cartilage by μmri. Magnetic Resonance in Medicine, 65(3), 656-663.

Raya, J. G. (2015). Techniques and applications of in vivo diffusion imaging of articular cartilage. Journal of Magnetic Resonance Imaging, 41(6), 1487-1504.

Sandra Camarero-Espinosa, Rothen-Rutishauser, B., Foster, E. J., & Weder, C. (2016). Articular cartilage: from formation to tissue engineering. Biomaterials Science, 4(5), 734-767.

Dodge, G. R. and Poole, A. R. (1989). Immunohistochemical detection and immunochemical analysis of type ii collagen degradation in human normal, rheumatoid, and osteoarthritic articular cartilages and in explants of bovine articular cartilage cultured with interleukin 1.. Journal of Clinical Investigation, 83(2), 647-661.

Zheng, S. and Xia, Y. (2010). Changes in proton dynamics in articular cartilage caused by phosphate salts and fixation solutions. Cartilage, 1(1), 55-64.

He, B., Wu, J., Kirk, T., Carrino, J. A., Chen, X., & Xu, J. (2014). High-resolution measurements of the multilayer ultra-structure of articular cartilage and their translational potential. Arthritis Research &Amp; Therapy, 16(2), 205.

Hunziker, E. B., Kapfinger, E., & Geiss, J. (2007). The structural architecture of adult mammalian articular cartilage evolves by a synchronized process of tissue resorption and neoformation during postnatal development. Osteoarthritis and Cartilage, 15(4), 403-413.

He, B., Wu, J., Chim, S. M., Xu, J., & Kirk, T. (2013). Microstructural analysis of collagen and elastin fibres in the kangaroo articular cartilage reveals a structural divergence depending on its local mechanical environment. Osteoarthritis and Cartilage, 21(1), 237-245.

Gao, J., Ren, P., & Gong, H. (2023). Morphological and mechanical alterations in articular cartilage and subchondral bone during spontaneous hip osteoarthritis in guinea pigs. Frontiers in Bioengineering and Biotechnology, 11.

Felisbino, S. L. and Carvalho, H. F. (2002). Ectopic mineralization of articular cartilage in the bullfrog rana catesbeiana and its possible involvement in bone closure. Cell and Tissue Research, 307(3), 357-365.

Gosset, M., Berenbaum, F., Thirion, S. and Jacques, C., 2008. Primary culture and phenotyping of murine chondrocytes. Nature protocols, 3(8), pp.1253-1260.

Onyango, I. G., Lu, J., Rodova, M., Lezi, E., Crafter, A., & Swerdlow, R. H. (2010). Regulation of neuron mitochondrial biogenesis and relevance to brain health. Biochimica Et Biophysica Acta (BBA) - Molecular Basis of Disease, 1802(1), 228-234.

Xu, D., Li, C., Jiang, Z., Wang, L., Huang, H., Z, L., … & Wang, T. (2020). The hypoglycemic mechanism of catalpol involves increased ampk-mediated mitochondrial biogenesis. Acta Pharmacologica Sinica, 41(6), 791-799.

Sheng, B., Wang, X., Su, B., Lee, H. G., Casadesús, G., Perry, G., … & Zhu, X. (2011). Impaired mitochondrial biogenesis contributes to mitochondrial dysfunction in alzheimer's disease. Journal of Neurochemistry, 120(3), 419-429.

Hwang, J., Kim, K. M., Oh, H. T., Yoo, G. D., Jeong, M. G., Lee, H., … & Hong, J. (2022). Taz links exercise to mitochondrial biogenesis via mitochondrial transcription factor a. Nature Communications, 13(1).

Popov, L. (2020). Mitochondrial biogenesis: an update. Journal of Cellular and Molecular Medicine, 24(9), 4892-4899.

Qi, X. and Wang, J. (2020). Melatonin improves mitochondrial biogenesis through the ampk/pgc1α pathway to attenuate ischemia/reperfusion-induced myocardial damage. Aging, 12(8), 7299-7312.

Ren, B., Zhang, T., Guo, Q., Che, J., Kang, Y., Cui, R., … & Shi, G. (2022). Nrf2 deficiency attenuates testosterone efficiency in ameliorating mitochondrial function of the substantia nigra in aged male mice. Oxidative Medicine and Cellular Longevity, 2022, 1-33.

Shao, C., Zhou, X., Miao, Y., Wang, P., Zhang, Q., & Huang, Q. (2021). In situ observation of mitochondrial biogenesis as the early event of apoptosis. iScience, 24(9), 103038.

Andrés, A., Bell, M. R., Ejiofor, S., Zurcher, G., Petersen, D. R., & Ronis, M. J. J. (2014). n-acetylcysteine inhibits the up-regulation of mitochondrial biogenesis genes in livers from rats fed ethanol chronically. Alcoholism: Clinical and Experimental Research, 38(12), 2896-2906.

Dong, W., Wang, F., Guo, W., Zheng, X., Chen, Y., Zhang, W., … & Hong, S. (2015). Aβ25–35 suppresses mitochondrial biogenesis in primary hippocampal neurons. Cellular and Molecular Neurobiology, 36(1), 83-91.

Bernard, K., Logsdon, N. J., Miguel, V., Benavides, G. A., Zhang, J., Carter, A. B., … & Thannickal, V. J. (2017). Nadph oxidase 4 (nox4) suppresses mitochondrial biogenesis and bioenergetics in lung fibroblasts via a nuclear factor erythroid-derived 2-like 2 (nrf2)-dependent pathway. Journal of Biological Chemistry, 292(7), 3029-3038.

Zhu, Z., Xu, L., Cao, D., Song, C., Wang, Y., Li, M., … & Xie, Z. (2021). Effect of orexin-a on mitochondrial biogenesis, mitophagy and structure in hek293-appswe cell model of alzheimer's disease. Clinical and Experimental Pharmacology and Physiology, 48(3), 355-360.

Lee, T., Kim, M. K., & Chong, Y. (2022). Promotion of mitochondrial biogenesis by synthetic 1,2- or 1,3-digallates through activation of an energy sensing network. Bulletin of the Korean Chemical Society, 43(3), 407-411.

Wang, X., Cai, B., Jia, Z., Chen, Y., Guo, S., Liu, Z., … & Hu, B. (2024). Mitostructseg: a comprehensive platform for mitochondrial structure segmentation and analysis.

Epand, R. M., Martinou, J., & Montessuit, S. (2003). Transbilayer lipid diffusion promoted by bax: implications for apoptosis. Biochemistry, 42(49), 14576-14582.

Yamashita, A., Fujimoto, M., Katayama, K., Yamaoka, S., Tsutsumi, N., & Arimura, S. (2016). Formation of mitochondrial outer membrane derived protrusions and vesicles in arabidopsis thaliana. Plos One, 11(1), e0146717.

Blanco, F., López-Armada, M., & Maneiro, E. (2004). Mitochondrial dysfunction in osteoarthritis. Mitochondrion, 4(5-6), 715-728.

Madhu, V. (2024). Opa1 protects intervertebral disc and knee joint health in aged mice by maintaining the structure and metabolic functions of mitochondria..

Marks, R. (2022). Knee joint neural pathways and their osteoarthritis pathogenic linkage implications. Acta Scientific Orthopaedics, 116-126.

Seeley, M., Lee, H., Son, S., Timmerman, M., Lindsay, M., & Hopkins, J. (2022). A review of the relationships between knee pain and movement neuromechanics. Journal of Sport Rehabilitation, 31(6), 684-693.

Heijink, A., Gomoll, A.H., Madry, H., Drobnič, M., Filardo, G., Espregueira-Mendes, J. and Van Dijk, C.N., 2012. Biomech

Wasser, J. (2023). Exploring relationships among multi-disciplinary assessments for knee joint health in service members with traumatic unilateral lower limb loss: a two-year longitudinal investigation. Scientific Reports, 13(1).

Cancedda, R., 2009. Cartilage and bone extracellular matrix. Current pharmaceutical design, 15(12), pp.1334-1348.

Kulyar, M. F., Mo, Q., Yao, W., Li, Y., Nawaz, S., Loon, K. S., … & Qi, D. (2024). Modulation of apoptosis and inflammasome activation in chondrocytes: co-regulatory role of chlorogenic acid. Cell Communication and Signaling, 22(1).

Bai, Y., Gong, X., Dou, C., Cao, Z. and Dong, S., 2019. Redox control of chondrocyte differentiation and chondrogenesis. Free Radical Biology and Medicine, 132, pp.83-89.

Mobasheri, A., Rayman, M.P., Gualillo, O., Sellam, J., Van Der Kraan, P. and Fearon, U., 2017. The role of metabolism in the pathogenesis of osteoarthritis. Nature Reviews Rheumatology, 13(5), pp.302-311.

Goldring, M. B. and Goldring, S. R. (2007). Osteoarthritis. Journal of Cellular Physiology, 213(3), 626-634.

Goldring, M. B. and Marcu, K. B. (2009). Cartilage homeostasis in health and rheumatic diseases. Arthritis Research &Amp; Therapy, 11(3), 224.

Issa, R. and Griffin, T., 2012. Pathobiology of obesity and osteoarthritis: integrating biomechanics and inflammation. Pathobiology of Aging & Age-related Diseases, 2(1), p.17470.

Lambrecht, S., Verbruggen, G., Elewaut, D., & Deforce, D. (2008). Differential expression of αb-crystallin and evidence of its role as a mediator of matrix gene expression in osteoarthritis. Arthritis &Amp; Rheumatism, 60(1), 179-188.

Rades, N., Licha, K., & Haag, R. (2018). Dendritic polyglycerol sulfate for therapy and diagnostics. Polymers, 10(6), 595.

Cornish, A. J., Filippis, I., David, A., & Sternberg, M. J. (2015). Exploring the cellular basis of human disease through a large-scale mapping of deleterious genes to cell types. Genome Medicine, 7(1).

Mainil-Varlet, P., Schiavinato, A., & Ganster, M. (2012). Efficacy evaluation of a new hyaluronan derivative hyadd®4-g to maintain cartilage integrity in a rabbit model of osteoarthritis. Cartilage, 4(1), 28-41.

Aigner, T. and McKenna, L. A. (2002). Molecular pathology and pathobiology of osteoarthritic cartilage. Cellular and Molecular Life Sciences (CMLS), 59(1), 5-18.

Salvat, C., Pigenet, A., Humbert, L., Bérenbaum, F., & Thirion, S. (2005). Immature murine articular chondrocytes in primary culture: a new tool for investigating cartilage. Osteoarthritis and Cartilage, 13(3), 243-249.

Eegher, S. v., Pérez-Lozano, M. L., Toillon, I., Valour, D., Pigenet, A., Citadelle, D., … & Houard, X. (2021). The differentiation of prehypertrophic into hypertrophic chondrocytes drives an oa-remodeling program and il-34 expression. Osteoarthritis and Cartilage, 29(2), 257-268.

Ratneswaran, A., Sun, M. M., Dupuis, H., Sawyez, C. G., Borradaile, N. M., & Beier, F. (2017). Nuclear receptors regulate lipid metabolism and oxidative stress markers in chondrocytes. Journal of Molecular Medicine, 95(4), 431-444.

Huang, H., Veien, E. S., Zhang, H., Ayers, D. C., & Song, J. (2016). Skeletal characterization of smurf2-deficient mice and in vitro analysis of smurf2-deficient chondrocytes. Plos One, 11(1), e0148088.

Tew, S.R., Murdoch, A.D., Rauchenberg, R.P. and Hardingham, T.E., 2008. Cellular methods in cartilage research: primary human chondrocytes in culture and chondrogenesis in human bone marrow stem cells. Methods, 45(1), pp.2-9.

Olivotto, E., Otero, M., Astolfi, A., Platano, D., Facchini, A., Pagani, S., … & Marcu, K. B. (2013). Ikkα/chuk regulates extracellular matrix remodeling independent of its kinase activity to facilitate articular chondrocyte differentiation. PLoS ONE, 8(9), e73024.

Kim, S. G., Song, J., Ryplida, B., Jo, H. J., Jeong, G., Kang, I. Y., … & Park, S. J. (2023). Touchable electrochemical hydrogel sensor for detection of reactive oxygen species-induced cellular senescence in articular chondrocytes. Advanced Functional Materials, 33(17).

Pérez-Lozano, M. L., Sudre, L., Eegher, S. v., Citadelle, D., Pigenet, A., Lafage-Proust, M., … & Houard, X. (2022). Gremlin-1 and bmp-4 overexpressed in osteoarthritis drive an osteochondral-remodeling program in osteoblasts and hypertrophic chondrocytes. International Journal of Molecular Sciences, 23(4), 2084.

Sun, M. M. and Beier, F. (2019). Liver x receptor activation regulates genes involved in lipid homeostasis in developing chondrocytes.

Geng, T., Li, P., Okutsu, M., Yin, X., Kwek, J., Zhang, M. and Yan, Z., 2010. PGC-1α plays a functional role in exercise-induced mitochondrial biogenesis and angiogenesis but not fiber-type transformation in mouse skeletal muscle. American Journal of Physiology-Cell Physiology, 298(3), pp.C572-C579.

Kan, S., Duan, M., Liu, Y., Wang, C. and Xie, J., 2021. Role of mitochondria in physiology of chondrocytes and diseases of osteoarthritis and rheumatoid arthritis. Cartilage, 13(2_suppl), pp.1102S-1121S.

Austin, S. and St-Pierre, J. (2012). Pgc1α and mitochondrial metabolism – emerging concepts and relevance in ageing and neurodegenerative disorders. Journal of Cell Science, 125(21), 4963-4971.

Rius-Pérez, S., Torres-Cuevas, I., Millán, I., Ortega, Á.L. and Pérez, S., 2020. PGC-1α, inflammation, and oxidative stress: an integrative view in metabolism. Oxidative medicine and cellular longevity, 2020(1), p.1452696.

Yang, Y.N., Zhang, M.Q., Yu, F.L., Han, B., Bao, M.Y., Li, X. and Zhang, Y., 2023. Peroxisom proliferator-activated receptor-γ coactivator-1α in neurodegenerative disorders: A promising therapeutic target. Biochemical Pharmacology, p.115717.

Osorio-Conles, Ó., Olbeyra, R., Moizé, V., Ibarzábal, A., Giró, O., Viaplana, J., … & Hollanda, A. d. (2022). Positive effects of a mediterranean diet supplemented with almonds on female adipose tissue biology in severe obesity. Nutrients, 14(13), 2617.

Guo, M., Zhang, J., Han, J., Hu, Y., Ni, H., Yuan, J., … & Li, N. (2024). Vegfr2 blockade inhibits glioblastoma cell proliferation by enhancing mitochondrial biogenesis. Journal of Translational Medicine, 22(1).

Villena, J.A., 2015. New insights into PGC-1 coactivators: redefining their role in the regulation of mitochondrial function and beyond. The FEBS journal, 282(4), pp.647-672.

Singh, B.K., Sinha, R.A., Tripathi, M., Mendoza, A., Ohba, K., Sy, J.A., Xie, S.Y., Zhou, J., Ho, J.P., Chang, C.Y. and Wu, Y., 2018. Thyroid hormone receptor and ERRα coordinately regulate mitochondrial fission, mitophagy, biogenesis, and function. Science signaling, 11(536), p.eaam5855.

Liang, H. and Ward, W. F. (2006). Pgc-1α: a key regulator of energy metabolism. Advances in Physiology Education, 30(4), 145-151.

Malik, N., Ferreira, B. I., Hollstein, P. E., Curtis, S. D., Trefts, E., Novak, S. W., … & Shaw, R. J. (2023). Induction of lysosomal and mitochondrial biogenesis by ampk phosphorylation of fnip1. Science, 380(6642).
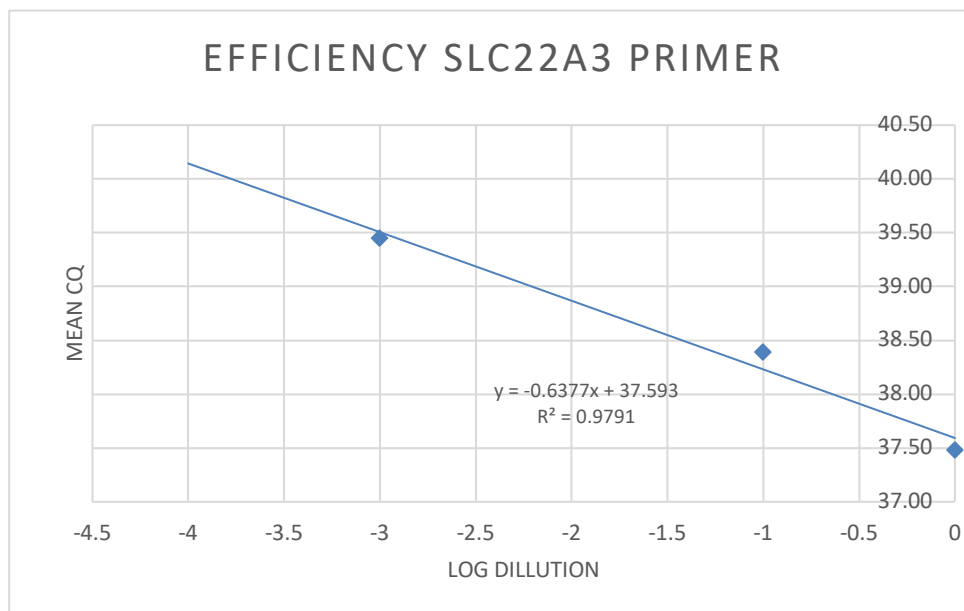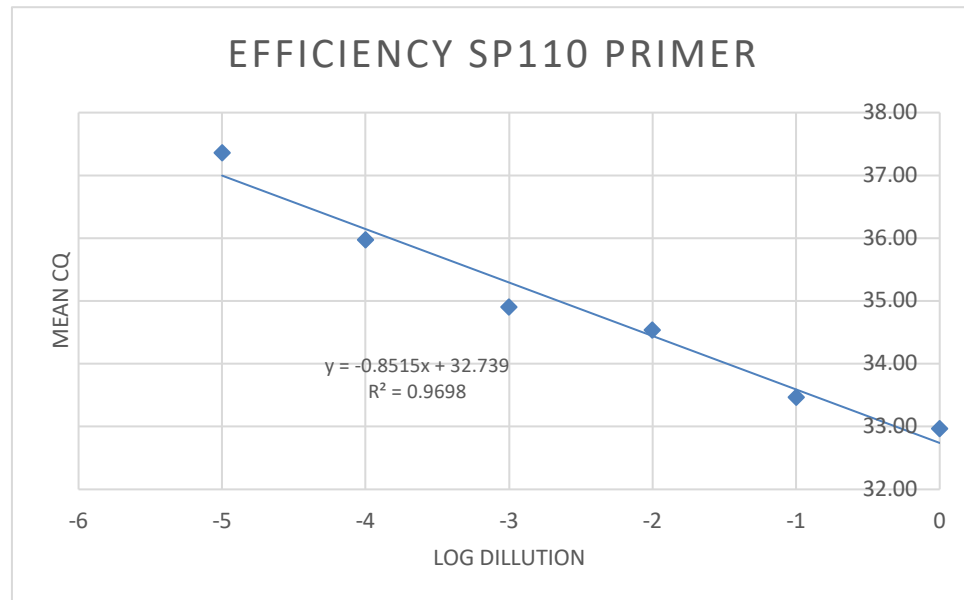
Abu Shelbayeh, O., Arroum, T., Morris, S. and Busch, K.B., 2023. PGC-1α is a master regulator of mitochondrial lifecycle and ROS stress response. Antioxidants, 12(5), p.1075.

Sharabi, K., Lin, H., Tavares, C. D., Dominy, J. E., Camporez, J. P., Perry, R. J., … & Puigserver, P. (2017). Selective chemical inhibition of pgc-1α gluconeogenic activity ameliorates type 2 diabetes. Cell, 169(1), 148-160.e15.

Xie, K., Wang, Y., Yin, L., Wang, Y., Chen, H., Mao, X. and Wang, G., 2021. Hydrogen gas alleviates sepsis-induced brain injury by improving mitochondrial biogenesis through the activation of PGC-α in mice. Shock, 55(1), pp.100-109.

Han, H. and Dong, Y. (2020). Dihydromyricetin protects against gentamicin-induced ototoxicity via pgc-1α/sirt3 signaling in vitro. Frontiers in Cell and Developmental Biology, 8.

Praharaj, P. P., Patra, S., Singh, A., Panigrahi, D. P., Lee, H. Y., Kabir, M. F., … & Bhutia, S. K. (2024). Clu (clusterin) and ppargc1a/pgc1α coordinately control mitophagy and mitochondrial biogenesis for oral cancer cell survival. Autophagy, 20(6), 1359-1382.

Lin, J., Handschin, C. and Spiegelman, B.M., 2005. Metabolic control through the PGC-1 family of transcription coactivators. Cell metabolism, 1(6), pp.361-370.

Xiang, Y., Fang, B., Liu, Y., Yan, S., Cao, D., Mei, H., Wang, Q., Hu, Y. and Guo, T., 2020. SR18292 exerts potent antitumor effects in multiple myeloma via inhibition of oxidative phosphorylation. Life Sciences, 256, p.117971.

Gerbec, Z. and Malarkannan, S., 2021. NK cell-mediated immunotherapy: The exquisite role of PGC-1a in metabolic reprogramming. In Successes and Challenges of NK Immunotherapy (pp. 121-142). Academic Press.

Wang, Y., Peng, J., Yang, D., Xing, Z., Jiang, B., Ding, X., Jiang, C., Ouyang, B. and Su, L., 2024. From metabolism to malignancy: the multifaceted role of PGC1α in cancer. Frontiers in Oncology, 14.

Button, K.S., Ioannidis, J.P., Mokrysz, C., Nosek, B.A., Flint, J., Robinson, E.S. and
    Munafò, M.R., 2013. Power failure: why small sample size undermines the
    reliability of neuroscience. Nature reviews neuroscience, 14(5), pp.365-376.

Liu, Y., Zhou, J. and White, K.P., 2014. RNA-seq differential expression studies: more
    sequence or more replication?. Bioinformatics, 30(3), pp.301-304.

Leek, J.T., Scharpf, R.B., Bravo, H.C., Simcha, D., Langmead, B., Johnson, W.E.,
    Geman, D., Baggerly, K. and Irizarry, R.A., 2010. Tackling the widespread and
    critical impact of batch effects in high-throughput data. Nature Reviews
    Genetics, 11(10), pp.733-739.

Appendices

EFFICIENCY SP110 PRIMER

y = -0.8515x + 32.739
R² = 0.9698

EFFICIENCY SLC22A3 PRIMER

y = -0.6377x + 37.593
R² = 0.9791

Supplement figure 1 Primer design efficiency test result

Sp110 and Slc22a3 didn't have visible off-target binding or primer dimers and had an optimal annealing temperature of 60°C. The efficiency and specificity of these primers were tested with a standard curve. R^2 were (a) 0.9608, and (b) 0.9791.
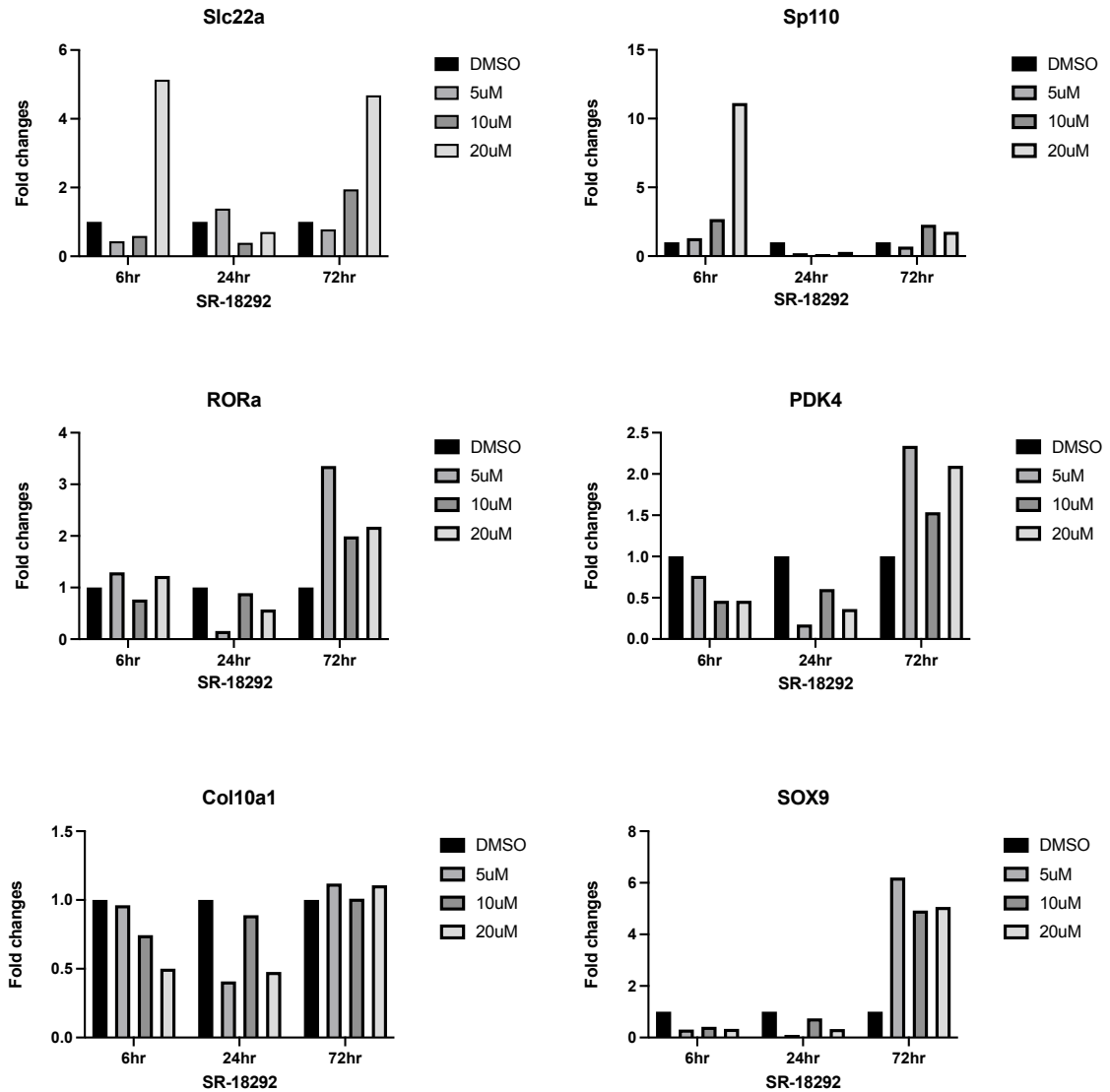
Supplement figure 2 qPCR result with selected genes from RNA-seq gene list

qPCR result with designed primers (Slc22a, Sp110) and four selected genes known as involved in the development, maintenance, repair, and metabolic processes of cartilage.

Supplement figure 3 PCA result of RNA-seq

PCA result include 4 trials (trial1, trial3, trial4, and trial5). Control of each trial is red and SR-18292 treatment is blue. There are more similarity within each trials rather than treatment compared to control. Control and treatment group of trial 1, trial 3, and trial 4 are gathered, while trial 5 showed different result.

Supplement figure 4 PCA result of RNA-seq

PCA result include 4 trials (trial1, trial3, trial4, and trial5). Control of each trial is red and SR-18292 treatment is blue. There are more similarity within each trials rather than treatment compared to control. Control and treatment group of trial 1, trial 3, and trial 4 are gathered, while trial 5 showed different result.

Supplement figure 5 PCA result of RNA-seq

PCA result include 4 trials (trial1, trial3, trial4, and trial5). Control of each trial is red and SR-18292 treatment is blue. There are more similarity within each trials rather than treatment compared to control. Control and treatment group of trial 1, trial 3, and trial 4 are gathered, while trial 5 showed different result.

Supplement figure 6 PCA result of RNA-seq

PCA result include 4 trials (trial1, trial3, trial4, and trial5). Control of each trial is red and SR-18292 treatment is blue. There are more similarity within each trials rather than treatment compared to control. Control and treatment group of trial 1, trial 3, and trial 4 are gathered, while trial 5 showed different result.

DEGS	Gene	FDR	P-value
UP	Cxcl13 (C-X-C motif chemokine ligand 13)	20.394	0.00146
	Grik4 (glutamate receptor, ionotropic, kainate 4)	12.305	0.00302
	Slc22a3 (solute carrier family 22 (organic cation transporter), member 3)	2.483	0.00590
	Pou2f2 (POU domain, class 2, transcription factor 2)	6.231	0.00749
DOWN	Pmaip1 (phorbol-12-myristate-13-acetate-induced protein 1)	-5.238	0.0112
	Sp110 (Sp110 nuclear body protein)	-1.870	0.0123
	Pla2g4b	-12.351	0.0319

Supplement figure 7 Gene ontology analysis of PGC1a target genes differentially expressed between control and SR-18292 treated cells.

Mitochondrial metabolism related protein coding genes with P-value < 0.05 were selected among 1494 genes that showed fold change >1.5 between control and SR-18292 treated group.

ID	Fold change	P-value
Tcea1-ps1	44.200	0.00005
Gm8752	38.600	0.00006
Gm9320	-1.760	0.00197
Gm9762	-2.130	0.00302
Gm12161	5.020	0.00329
Gm16555	3.500	0.00564
Gm5776	-3.300	0.00586
Gm5564	-3.860	0.00707
Gm48944	4.500	0.00735
Eef1ece2	-1.600	0.00749
Serpina3h	16.000	0.00766
Snora68	-7.140	0.00811
Ptma-ps2	-1.820	0.00841
Gm24888	-2.560	0.00864
Oprd1	2.300	0.01120
Sp110	-1.870	0.01230
Mpo	-2.720	0.01280
Rps15a-ps6	1.860	0.01410
2310002F09Rik	1.990	0.01480
Ighm	-3.480	0.01560
Gm6916	-1.710	0.01590
Gm25313	-1.810	0.01740
Gm5417	-15.300	0.01760
4632433K11Rik	-6.470	0.01800
mt-Td	-1.900	0.01830
Gm47926	-5.980	0.01930
Gm19195	4.170	0.02080
Gm38155	-2.300	0.02080
Asb2	2.870	0.02090
Gm12168	-4.200	0.02090
Gm13237	-2.900	0.02190
9930111J21Rik1	-1.940	0.02240
Grtp1	1.610	0.02280
Itpa-ps1	3.720	0.02310
Gm16433	6.240	0.02320
Nyx	-1.650	0.02320
Slc25a2	2.170	0.02650
Spaar	-1.940	0.02660
Gm44775	3.080	0.02770
Gm20689	-25.900	0.02820
2410039M03Rik	-1.890	0.02920
Serpina3m	1.970	0.03100

Gm15801	-16.600	0.03230
Gm8783	-16.600	0.03230
Idi1-ps1	-20.300	0.03240
Doc2b	2.490	0.03290
Gm5259	-6.780	0.03300
Gm25541	-1.530	0.03370
Gja8	-2.140	0.03440
Gm13241	1.770	0.03440
Gm15454	8.160	0.03460
Gm4617	-2.050	0.03600
Gm12250	-2.730	0.03620
Gm5879	-2.870	0.03680
Gm28979	-3.780	0.03770
Gm9795	-31.600	0.03780
Zfp980	-2.550	0.03780
Gm35082	1.890	0.03810
Pdcd5-ps	3.980	0.03830
Gm50255	-3.030	0.03850
Gm47950	-2.860	0.03930
Gm37855	-1.970	0.03980
Gm25184	-7.550	0.04140
Gm50169	-1.730	0.04220
Rpl21-ps15	4.630	0.04260
Gm21182	-2.830	0.04360
Gm49893	-5.760	0.04360
Gm31374	1.880	0.04420
Gm10390	-3.250	0.04480
Gm44939	2.890	0.04540
Tex26	2.080	0.04540
Gm13288	-2.210	0.04590
Gm15421	-2.900	0.04600
Semp2ll	2.900	0.04600
Gm25099	-1.590	0.04640
Rsph10b	-1.680	0.04710
C230031I18Rik	1.560	0.04740
Gm42421	4.520	0.04740
Snord14d	-5.750	0.04760
Gm12184	-1.730	0.04880
Zfp335os	-1.700	0.04900
Gm44280	-4.000	0.05000

Supplement figure 8 All significantly changed genes in SR-18292 treated group compared to control

Among 1494 genes showed fold change < 1.5, 82 genes were selected based on p value < 0.05. All 82 genes with their fold change and p value were shown in table. These genes were used to analyze expression changes in treatment group compared to control.

Curriculum Vitae

Name: Yuri Kim

Post-secondary   Ewha Womans University
Education and   Seoul, Korea
Degrees: 2018-2022 B.A.

                        The University of Western Ontario
                        London, Ontario, Canada
                        2022-2024 M.A.

Honours and   Western Graduate Research Scholarship (WGRS)
Awards: 2022-2024

Related Work   Teaching Assistant
                        (Department of Physiology and Pharmacology)
Experience   University of Western Ontario
                        2022-2024

Publications: